Chem Soc Rev

Cite this: *Chem. Soc. Rev.*, 2012, **41**, 7085–7107

www.rsc.org/csr

CRITICAL REVIEW

Molecularly-mediated assemblies of plasmonic nanoparticles for Surface-Enhanced Raman Spectroscopy applications

Luca Guerrini and Duncan Graham*

Received 3rd April 2012
DOI: 10.1039/c2cs35118h

In recent years, Surface-Enhanced Raman Spectroscopy (SERS) has experienced a tremendous increase of attention in the scientific community, expanding to a continuously wider range of diverse applications in nanoscience, which can mostly be attributed to significant improvements in nanofabrication techniques that paved the way for the controlled design of reliable and effective SERS nanostructures. In particular, the plasmon coupling properties of interacting nanoparticles are extremely intriguing due to the concentration of enormous electromagnetic enhancements at the interparticle gaps. Recently, great efforts have been devoted to develop new nanoparticle assembly strategies in suspension with improved control over hot-spot architecture and cluster structure, laying the foundation for the full exploitation of their exceptional potential as SERS materials in a wealth of chemical and biological sensing. In this review we summarize in an exhaustive and systematic way the state-of-art of plasmonic nanoparticle assembly in suspension specifically developed for SERS applications in the last 5 years, focusing in particular on those strategies which exploited molecular linkers to engineer interparticle gaps in a controlled manner. Importantly, the novel advances in this rather new field of nanoscience are organized into a coherent overview aimed to rationally describe the different strategies and improvements in the exploitation of colloidal nanoparticle assembly for SERS application to real problems.

Centre for Molecular Nanometrology, WestCHEM, Pure and Applied Chemistry, University of Strathclyde, 295 Cathedral Street, Glasgow, G1 1XL, UK. E-mail: duncan.graham@strath.ac.uk; Fax: +44 (0)141 552 0876; Tel: +44 (0)141 548 4701

Introduction

Electromagnetic interaction of light with nanoscale metals can generate collective oscillations of conduction electrons generally known as localized surface plasmon resonances (LSPRs).[1–3] This unique ability of nanostructured metals to manipulate

Luca Guerrini

Luca Guerrini achieved his Master's degree cum laude in Industrial Chemistry from University of Bologna, Italy. In 2009, he received his PhD from Universidad Autónoma de Madrid, Spain, for his work on functionalization of metal substrates for the engineering of SERS-based nanosensors for trace detection of persistent organic pollutants. His thesis was awarded the ''Premio Extraordinario de Doctorado, 2009''. He is currently a post-doctoral fellow at the Centre for Molecular Nanometrology in the University of Strathclyde where his research mainly focuses on development of SERS substrates for bio-sensing applications.

Duncan Graham

Duncan Graham is Research Professor of Chemistry and Director of the Centre for Molecular Nanometrology at the University of Strathclyde in Glasgow. He is currently Director of WestCHEM and he has been awarded numerous awards for his research including a Royal Society Wolfson Research Merit award (2010). He is also a cofounder and director of Renishaw Diagnostics Ltd (2007). He completed a PhD in organic chemistry at the University of Edinburgh (1996) and now his interests are in using synthetic chemistry to produce nanosensors that respond to a specific biological species or event as measured by surface enhanced Raman scattering.

light–matter interactions at the nanometer scale, generating high local enhancements of the electromagnetic energy, paved the way for the development of new fundamental research and increasing numbers of novel technological applications, which span from surface-enhanced spectroscopies,[4–10] to catalysis,[11,12] plasmonic solar cells,[13] nanodevices for bio-applications,[14,15] photoacoustic imaging[16] and beyond.

Plasmonic resonances in noble metal nanostructures (Ag and Au) occur at frequencies corresponding to typical electronic excitations in matter. The resulting coupling between the LSPRs of the nanostructures and the EM fields emitted by molecules located in close proximity to the metal surface is at the heart of the dramatic modification of the molecular radiative properties[17] such as the huge enhancement of the Raman scattering (surface-enhanced Raman scattering, SERS). Additionally, assembly of individual plasmonic nanoparticle building blocks into plasmonic 'molecules' generates nanostructures with new or enhanced optical performances[18] as a result of the near-field coupling between individual LSPRs of the adjacent nanoparticles which concentrates high electromagnetic fields at the interparticle gap. Raman scatterers located at the interparticle junctions may experience SERS enhancement that exceeds that of the isolated nanoparticles by several orders of magnitude[19] enabling the detection of single molecules.[20–23]

Since its initial discovery more than 30 years ago,[24,25] SERS showed great potential as an extremely powerful analytical technique and tool for fundamental surface studies but its wide development outside the spectroscopy community was largely hampered by the inherent irreproducibility associated with substrate fabrication methods. In the last decade, however, spectacular advances in nanofabrication techniques and deeper fundamental understanding of the phenomenon stimulated an exponential increase of SERS applications which nowadays have expanded across many fields of science.[5,7,26–39] Development of rationally designed SERS substrates with optimized, uniform and reproducible response has been explored *via* both top-down approaches, which involved a large number of nanolithography techniques to pattern complex nanostructures on a surface,[40–43] and bottom-up methods, which are usually based on chemically synthesized nanoparticles which can be further assembled in suspension or onto well-defined arrays on a substrate.[44–48]

In particular, Au and Ag nanoparticles with tunable plasmonic properties synthesized *via* wet chemical methods represented likely the most widespread source of SERS substrates. In this regard, in recent years there has been a growing effort to engineer interparticle junctions within rationally designed architectures of plasmonic colloidal nanoparticles with reproducible high SERS performance.

Recent excellent reviews extensively described the plasmon coupling effect in interacting nanoparticle structures[18] and provided an overview of the different approaches to control the assembly of plasmonic nanoparticles by colloid chemistry,[49] together with brief summaries of the SERS applications.

The purpose of this review is to summarize in a more exhaustive and systematic way the state-of-art of plasmonic nanoparticle assembly in suspension specifically developed for SERS applications in the last 5 years or less. Importantly, the novel advances in this rather new field of nanoscience are organized into a coherent overview aimed to rationally describe the different strategies and improvements in the exploitation of colloidal nanoparticle assembly for SERS application to real problems. Before that, the first part of the review builds the general background and rationale for providing all readers with the necessary experimental and theoretical tools needed for the full understanding and the development of critical thinking about the topic.

From normal Raman to SERS

The Raman effect is associated to the inelastic scattering of photons from a molecular system (*i.e.* simultaneous absorption of an incident photon and emission of another photon with different energy).[50] In fact, whereas most of the scattered photons conserve the same energy of the incident ones (Rayleigh scattering), a small fraction of them is scattered either at higher (anti-Stokes Raman scattering) or lower (Stokes Raman scattering) energy. The "modulation" of the photon energy corresponds to the energy difference between vibrational states in the molecule and the collection of the scattered photons (Raman bands) forms the Raman spectrum which constitutes the spectroscopic vibrational fingerprint of the investigated molecule.[50,51] Under typical conditions, anti-Stokes bands are much weaker and thus most of the Raman studies ignore this part of the Raman spectrum (Fig. 1b).

Importantly, due to the intrinsic nature of the Raman effect, Raman measurements can be carried out over a wide spectral range, usually from UV to near-infrared excitation frequencies, for any sort of molecular system. As a result, Raman spectroscopy is characterized by an extreme experimental flexibility which, for instance, lacks in other analytical techniques such as fluorescence spectroscopy where the choice of the excitation frequency is strictly limited by the optical properties of the specific fluorescent analyte. This, together with the extremely rich chemical and structural information provided by the Raman spectrum, promoted the application of Raman spectroscopy in many fields, such as art and heritage, materials science, biomedical and pharmaceutical studies, chemical sensing, vibrational studies and forensic science.[52–54] However, except for special cases of resonating molecules (Resonance Raman, RR), the inherent weakness of the Raman signal represents a severe limitation to the investigation of materials in low concentrations (*e.g.*, self-assembled monolayers, ultra-thin polymer films, nanomolar analyte solutions).

In 1977, three years after the initial observation by Fleischmann *et al.*[55] of an unexpected large Raman scattering from pyridine adsorbed on electrochemically roughened silver, Jeanmaire and Van Duyne[24] and Albrecht and Creighton[25] independently demonstrated that the presence of noble metal substrates (usually, gold or silver) with nanostructured features is at the origin of the dramatic signal enhancement. Their discovery paved the way for new applications of the Raman technique in the new terms of Surface-Enhanced Raman Spectroscopy (SERS). The SERS technique combines the intrinsic characteristic structural specificity and high flexibility of Raman spectroscopy with the extremely high sensitivity, with potential detection limits down to the single molecule,[6,20,21]

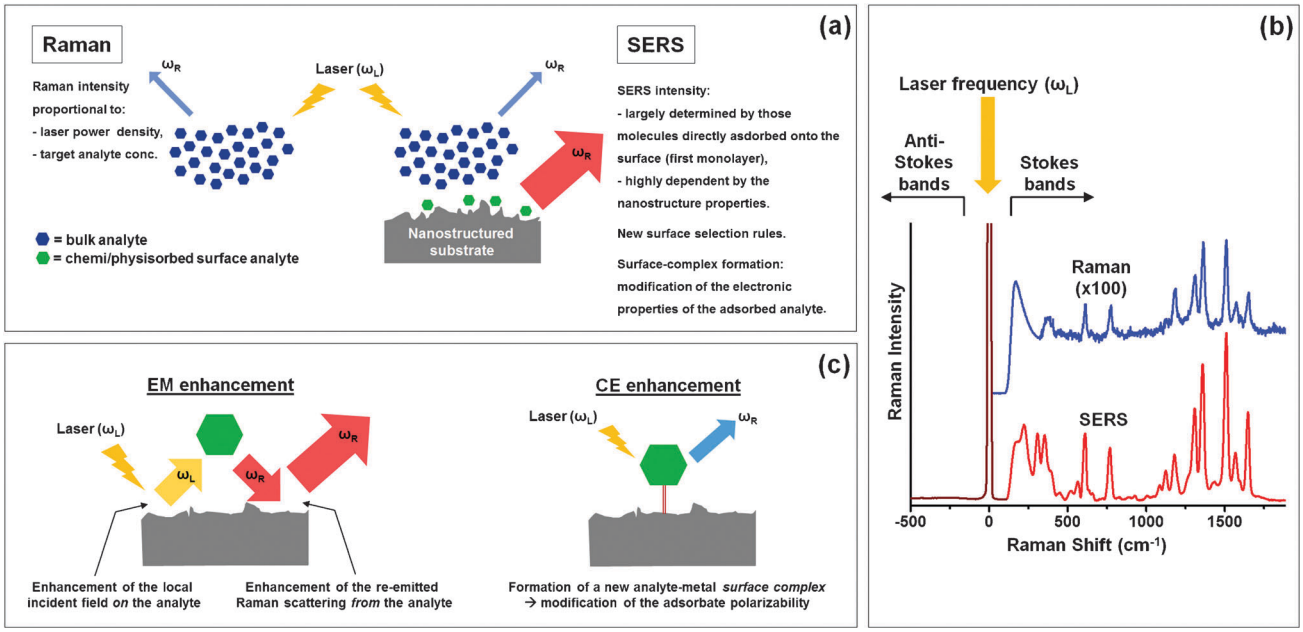

Fig. 1 (a) Schematic comparative visualization of the Raman and SERS phenomena. (b) SERS spectrum of Rhodamine 6G 10^{-7} M in silver hydroxylamine colloid (red line) and normal Raman spectrum of Rhodamine 6G 10^{-3} M in milli-Q water (blue line) multiplied by a factor of 100. The spectra were acquired using a 633 nm laser line under the same experimental conditions. (c) Schematic outline of the electromagnetic and chemical enhancements in SERS.

provided by the metal nanostructure amplification of the optical signal.

However, it must be underlined that the SERS phenomenon is not just a mere amplification of the Raman signal, but it is the final result of multiple factors, whose relative contribution to the observed SERS spectrum is case specific.[56] In fact, in normal Raman spectroscopy, the average Raman intensity is directly proportional to the laser power density and to the concentration of a target analyte with its specific Raman cross-section (*i.e.* scattering efficiency of a specific molecule for a given excitation wavelength[50]). This linear relationship can be translated to SERS only under specific conditions (for a given spot and at full monolayer coverage, the SERS signal is laser power dependent) and, in general, the presence of the nanostructure introduces a much greater degree of complexity into the experiment, which is mainly related to the metal substrate properties. In addition, several other phenomena, such as new 'surface selection rules' and surface complex formation, may contribute to a drastic alteration of the SERS spectral profile with respect to the original normal Raman spectrum. A visualization of the Raman and SERS phenomena is schematically outlined in Fig. 1a and b.

Recently, two books "Principles of Surface-Enhanced Raman Spectroscopy" by Le Ru and Etchegoin[51] and "Surface-enhanced Vibrational Spectroscopy" by Aroca[56] have finally provided a complete coherent overview of the principles of SERS, providing newcomers to the field with a progressive introduction to the complexity of this powerful technique and with the tools required to tackle the more specialized literature. Additionally, several sharp reviews[7,30,34,35,38,39,57–65] detail recent developments of SERS applications over a broad range of different fields and related topics.

In this review, we will report only selected, and sometimes 'simplified', principles related to the theory behind SERS spectroscopy which we believed strictly necessary for the interpretation of the latest research results in the controlled assembly of plasmonic nanoparticles for SERS applications.

Nowadays, it is widely accepted that the SERS enhancement can be considered as the result of two multiplicative effects:

The electromagnetic enhancement (EM)

The EM enhancement is the dominant contribution to dramatic enhancement of the signal in SERS and can be as high as $\sim 10^{10}$–10^{11}.[66] The existence of EM enhancement constitutes the indispensable condition to observe the SERS effect and its origin lies on the large local field enhancements that apply to a molecule located close to or at nanostructured surfaces when LSPRs are excited *via* electromagnetic interaction of light with metals. Therefore, the nature of the EM enhancement is strictly related to the nanostructure properties (size, shape and intrinsic dielectric property of the metal) and indifferently applies to all analytes.[51,56,67] The frequency and intensity of a plasmon resonance are also affected by the dielectric constant of the surrounding medium in contact with the metal. For the sake of easy understanding, local field enhancements at the metal surface can be imagined to produce two separate multiplicative effects on the Raman scattering: the first one, results from the enhancement of the local incident field *on* the analyte, whereas the second contribution is due to the enhancement of the re-emitted Raman scattering *from* the analyte (Fig. 1c). In the common $|E|^4$ approximation for zero-Stokes shift (*i.e.* excitation frequency, ω_L, $\approx$ Raman scattering frequency, ω_R; see ref. 68 for more details), the EM enhancement factor 'felt' by a single molecule located at a specific point

on the nanostructured surface (Single-Molecule EF, SM-EF) at the excitation frequency ω_L, is given by the expression:

$$SM - EF = \frac{|E_{Loc}(\omega_L)E_{Loc}(\omega_R)|^2}{|E_{Inc}|^4} \approx \frac{|E_{Loc}(\omega_L)|^4}{|E_{Inc}|^4} \quad (1)$$

where E_{Inc} and E_{Loc} are, respectively, the incident field on the nanostructure and the local field at the analyte. Importantly, the local field enhancement decreases rapidly when increasing the distance d from the surface with a decay $\sim 1/(a + d)$,[12] in the case of a sphere of radius a.[51] In addition, the tangential and normal components of the local field have different strength and their relative ratio is frequency dependent. This gives rise to a new set of 'surface selection rules' for a Raman scatterer adopting a fixed orientation at the metal surface that may result in the appearance of new Raman modes and changes in relative intensities of the spectral bands as compared to the normal Raman conditions.[56,67,69,70]

Despite the large interest that Single-Molecule SERS detection (SM-SERS) has gained in the last few years,[6,22,62,71–73] most of the practical SERS applications focus on obtaining averaged signals from a relatively high number of scatterers (average-SERS) at the metal surface. As a result, the average SERS regime normally offers higher signal reproducibility and stability making it suitable, for instance, for reliable quantitative analysis. On the other hand, lower enhancement factors (usually in the 10^5–10^7 range) are achieved as compared to those observed for single or few molecules located at the hot spots of highly active SERS nanostructures ($\sim 10^{10}$ and higher).[51,56] Therefore, rather than determining the local enhancement at a specific position on the surface (which is often a difficult task to perform), more useful information for average SERS applications is provided by the average-EF of the SERS substrate (AS-EF). AS-EF can be defined as:[51]

$$AS - EF = \frac{I_{SERS}/N_{Surf}}{I_{RS}/N_{Vol}} \quad (2)$$

where I_{RS} and I_{SERS} are, respectively, the Raman intensity for an average number N_{Vol} of molecules in the scattering volume, Vol, and the SERS intensity for an average number N_{Surf} of molecules adsorbed in the sub-monolayer range onto the metal surface in the same scattering volume. It is important to stress that the calculated AS-EF is highly dependent on several other parameters beside the metallic nanostructure properties and surface coverage, such as excitation frequency, experimental set-up and the chosen Raman molecule. This causes a fair degree of confusion when the SERS efficiency of a particular substrate is calculated and the comparison between EFs reported in the literature is often unreliable.[51]

The chemical enhancement (CE)

This second multiplicative contribution to the SERS enhancement relies on the modification of the Raman polarizability tensor of those molecules chemically adsorbed onto the nanostructure as a consequence of the formation of new analyte–metal surface complexes[67] (Fig. 1c). The resulting alteration of the electronic properties of the adsorbed analyte may allow new electronic transitions within the surface complex analogous to those observed for Resonant Raman scattering[50] which, in a similar manner, determine an increase of the Raman cross-section (in particular for those vibrations involved in the electronic transitions). Therefore, the CE is not related to the SERS process itself but to the modification of the adsorbate polarizability.[51,67] However, CE, when present, usually contributes to the overall enhancement to a much lesser extent (usually by 1–2 orders of magnitude) and, contrary to EM, is analyte-dependent.[56]

SERS substrates and general SERS application strategies

The theoretical and experimental studies showed that SERS-active substrates must possess nanostructured features of size much smaller than the wavelength of the exciting radiation, usually in the 10–80 nm range. For this reason, the SERS process would be better described as nanostructured-enhanced Raman scattering rather than simply surface-enhanced. In fact, when the size of the nanostructure becomes too large, the plasmonic resonance is strongly damped due to surface scattering of the conduction electrons (energy is lost through scattering). On the other hand, too small structures poorly support the plasmon resonances, and their optical response starts diverging from the pseudo bulk-plasmon behavior leading to low SERS enhancements.[30,51,56]

Noble metals such as gold and silver are the most widely employed materials for SERS substrates since they provide broad and intense plasmon resonances in the visible-near infrared region (the wavelength range of interest for Raman). In particular, silver can provide significantly larger SERS enhancements since gold is characterized by a large plasmon damping below ~ 600 nm which limits its use to the near-infrared region.[51] On the other hand, gold offers higher performance in terms of stability against oxidation, ease of preparation and surface modification and toxicity.[74]

Initially, the lack of nanofabrication methods capable of designing SERS substrates with the required reproducibility, homogeneity and high enhancement factors significantly hindered the impact of SERS in the scientific community for many years after its initial discovery.[75] In the last decade, however, important advances in nanofabrication techniques managed to overcome many of the previous limitations turning SERS into one of the most promising incisive analytical methods for biochemical detection and analysis.[7,30,35,37,76,77] In fact, since the first observation of Raman enhancement of pyridine molecules adsorbed on roughened silver electrodes,[55] an increasingly huge number of novel SERS substrates fabricated with a large variety of methods have been continuously appearing in the literature. We can arbitrarily group them into two main classes:

(1) Individual nanoparticles and their assemblies in dispersion.

(2) Structured surfaces, which are usually patterned either *via* lithographic techniques[42,78] or fabricated by depositing nanoparticles into highly ordered arrays on solid supports.[45,79]

In particular, the first class of materials offers effective SERS substrates where interparticle gaps can be tuned at the nanometer level *via* low cost and facile fabrication methods and allows easy chemical functionalization of the metal surface.

On the other hand, the second class of SERS substrates provides in general higher performances in terms of robustness, together with better enhancement reproducibility and uniformity.[29] In recent years, great effort has been put into developing new nanoparticle assembly strategies in dispersion with improved control over cluster geometry and SERS performance, and extending their use to a larger number of practical applications. In this review we intend to summarize, in an organic way, the recent progress in engineering interparticle junctions in nanoparticle clusters in suspension to yield high and reproducible enhanced fields *via* self-assembly methods, and their exploitation in a wealth of SERS applications.

For an extended overview of the most interesting advances in the very active field of SERS substrate engineering, the reader could refer to some excellent reviews such as Ko *et al.*,[30] Camden *et al.*,[75] and Banholzer *et al.*[80]

In this regard, it is worth however highlighting that a universal SERS substrate does not exist but the selection or the design of a specific nanostructure with its characteristic plasmonic properties is strictly linked to the nature of its final application. Similarly, the choice of specific experimental conditions (such as laser excitation wavelength, the detection set-up...) and the appropriate chemical functionalization of the metal surface to impart selectivity and sensitivity for specific target analytes also need consideration.

For instance, the first simple criterion that needs to be applied to the design of the optimum SERS substrate for a specific application is determination of the analytical regime of the experiment.[56] If a reliable quantitative analysis of a large ensemble of target molecules is required (average-SERS regime), the SERS nanostructure is usually engineered to provide relatively moderate (10^5–10^8) but highly reproducible and uniform enhancements. Otherwise, when the final goal of the SERS application is the detection of ultralow concentration (single/few molecules SERS regime), the nanostructured substrate is tailored to provide much higher enhancements (up to $\sim 10^{11}$)[51] which are usually achieved to the detriment of signal reproducibility.

Once the SERS regime of operation has been identified, it is possible to recognize two main strategies in the application of SERS to real problems:

Intrinsic SERS

The final goal of this strategy is to obtain the characteristic SERS spectrum of the target analyte. In the case of analytes which do not show sufficient affinity toward the metal and are therefore not capable of getting in close proximity to the nanoparticle, appropriate chemical functionalization of the surface is usually carried out to increase both sensitivity and selectivity toward the target analyte. For instance, 'molecular containers' such as calix[*n*]arenes, cyclodextrins and cucurbit[*n*]urils have been anchored on nanoparticle surfaces to promote, *via* host–guest interactions, the selective concentration and thus detection of hydrophobic pollutants such as polycyclic aromatic hydrocarbons (PAHs)[81–83] or other molecules with low or no affinity to the SERS-substrate, such as ferrocene.[84]

Extrinsic SERS

In this case, the detection of the analyte is indirectly achieved by monitoring the alteration of the SERS signal of Raman reporter molecules attached to the metal surface which is designed to be sensitive to the presence of the specific target or to changes in the local environment due to molecular events. Broadly speaking, we can classify the alterations of the SERS spectrum of the Raman reporter into:

(1) Change of the spectral profile

A clear example is the detection of non-Raman active species, such as atomic ions, by monitoring changes in the vibrational profile of chemoselective receptors at the metal surface after their complexation with the target ions.[85–87] For instance, Fig. 2a illustrates the detection scheme for chloride

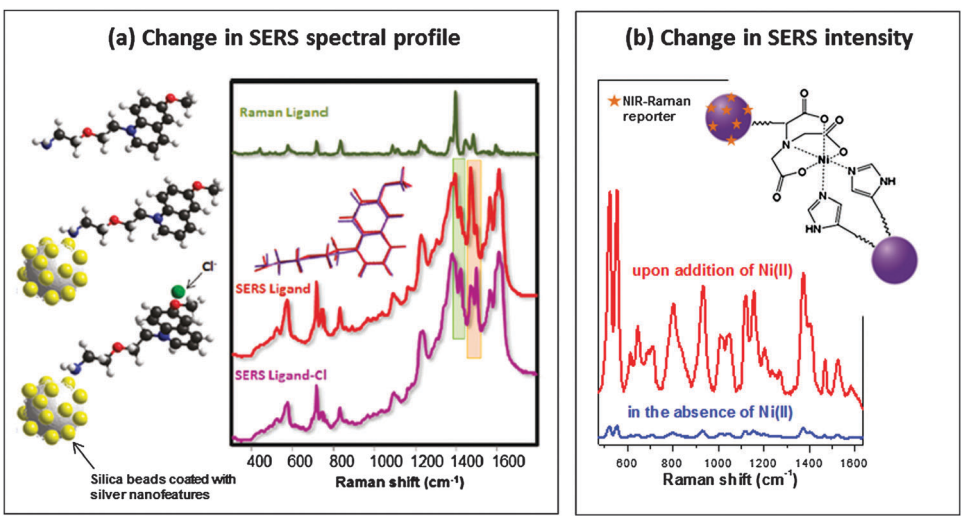

Fig. 2 Examples of *extrinsic SERS strategies*. (a) Silica beads coated with silver nanofeatures were functionalized with a Raman ligand whose molecular structure changes in the presence of chloride, as indicated by changes in the ligand SERS spectral profile. Reprinted with permission from ref. 87. Copyright 2011, American Chemical Society. (b) Aggregation of the nanoparticles is caused by formation of the octahedral complex when Ni(II) is coordinated between NTA and histidine moieties present at the particle surface. This results in the intensity increase of the SERS signal of the Raman reporter. Adapted with permission from ref. 90. Copyright 2012, John Wiley and Sons, Ltd.

ions by monitoring the vibrational changes occurring at a specific chemoselective receptor adsorbed on a silver-coated silica microbead, as reported by Tsoutsi *et al.*[87] Similarly, 4-mercapto benzoic acid (4-MBA) functionalized nanoparticles have been used as a pH-sensor[88,89] exploiting the high sensitivity of the carboxylate vibrational bands to changes in local pH.

(2) Change of the SERS intensity

In this case, the Raman reporter encoded on the nanostructure simply acts as a source of strong SERS signal whose intensity has been designed to selectively vary in the presence of the target analyte. For instance, metal ions such as Ni(II) have been detected down to the ppb range by designing dye-labeled gold nanoparticles functionalized with molecular ligands showing high affinity and selectivity for the target ion. As a result, selective nanoparticle aggregation occurs in the presence of Ni(II) leading to a marked increase of the SERS intensity[90] (Fig. 2b).

Dyes are organic molecules containing a chromophore group with absorption bands in the visible spectral region. When the laser excitation energy is close or coincident with that of an electronic transition within the chromophore, the Raman scattering is amplified by several orders of magnitude (Resonant Raman scattering, RRS) resulting in a multiplicative contribution to the EM enhancement.[56] The combination of SERS and RRS is usually referred to as SERRS (Surface-enhanced Resonant Raman Scattering). Thus, under resonant conditions, dye-labeled nanostructures (indicated in a variety of ways such as SERRS-encoded substrates, SERRS-tags, SERRS-probes, SERRS-labels, *etc.*) are characterized by both extreme sensitivity and a high degree of multiplexing capability due to the sharper vibrational bands of the dye Raman signature.[61,63]

Individual nanoparticles

Gold and silver colloids certainly represent the most common type of SERS-active materials. In particular, spherical or spherical-like nanoparticle dispersions are easily and reproducibly prepared *via* chemical reduction in solution, such as the well-known Lee and Meisel method[91] where the reducing agent (sodium citrate) acts also as stabilizing agent by adsorbing onto the metal surface and avoiding nanoparticle aggregation through electrostatic repulsions.

In the size range of interest for SERS, isolated spherical silver and gold nanoparticles in dispersion provide plasmon resonances in the spectral range of $\sim$380–420 nm and $\sim$515–550 nm, respectively (the bigger the nanoparticle, the more red-shifted and broadened is the plasmon resonance).[51] As previously mentioned, gold nanostructures are characterized by a marked optical absorption at wavelengths $<$600 nm, which leads to a strong damping of their plasmon resonances, and therefore of their enhancing ability, in this spectral region. On the other hand, monodispersed silver nanoparticles can provide much higher EM enhancements (in the order of AS-EF $\sim 10^4$–10^5)[51] but only for excitation laser matching the plasmonic resonance maximum in the unfavorable spectral range close to the UV. As a result, either the intrinsic optical property of the metal or the limited LSPR tunability *via* diameter modification limits the application of isolated spherical nanoparticles as SERS substrates.

Contrary to the size aspect, it is the shape feature of the individual nanoparticle that offers the most powerful tool to tailoring and fine-tuning its optical resonance properties[92] and, therefore, its EM enhancement ability. In fact, when the simple geometry of the sphere is remodeled into asymmetric features, new surface plasmon resonances arise in the extinction spectrum that can be tuned in a much wider spectral range. This is particularly important for gold, since it allows the LSPR to be red-shifted beyond the critical 600 nm threshold where the EM enhancing properties of gold approach that of silver. Moreover, the existence of corners or tips at the nanoparticle surface generates additional high local EM enhancements at these specific points of the surface (this phenomenon is known as the "lightning rod effect").[1] For instance, gold nanorods (GNRs) have attracted enormous interest as a SERS substrate,[93–95] in particular for *in vivo* imaging applications.[96] Their anisotropic shape allows their strong longitudinal LSPR to be tuned in a wide range of the near-infrared region in a highly controllable manner by varying their aspect ratio[97] (Fig. 3). GNRs of controlled size and aspect ratios are usually synthesized by anisotropic growth of gold nanosphere seeds in the presence of the surfactant cetyl trimethyl-ammonium bromide (CTAB) as a shape-directing agent.[97] The anisotropic shaping of the gold sphere splits the plasmonic response into two well-separated resonances: a damped blue-shifted transverse mode, and an intense red-shifted longitudinal mode. The latter plasmonic resonance is the most important for SERS applications since it is associated with maximum local EM enhancements at the tips of the GNRs which can exceed by up to several orders of magnitude those located on the single sphere surface.[1,17]

The strong dependence of the plasmon resonance wavelength on the nanoparticle shape has been exploited to synthesize a large number of different SERS-active nanostructures in addition to rods, such as cubes,[98,99] plates,[100] rings,[101] stars,[102,103]

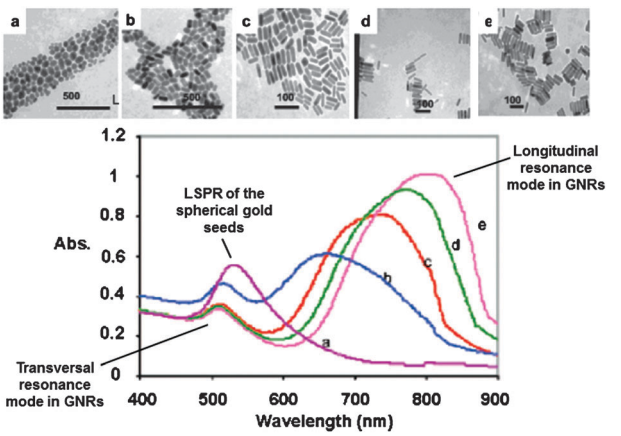

Fig. 3 Transmission electron micrographs and extinction spectra of Au nanorods of various aspect ratios. The seed sample has an aspect ratio of 1. Samples a, b, c, d, and e have aspect ratios of 1.35 $\pm$ 0.32, 1.95 $\pm$ 0.34, 3.06 $\pm$ 0.28, 3.50 $\pm$ 0.29, and 4.42 $\pm$ 0.23, respectively. Adapted with permission from ref. 216. Copyright 2005, American Chemical Society.

triangles,[104] nanoshells,[105–108] bipyramids,[109] nanoflowers[110] and worms[111] with unique plasmonic signatures and improved SERS performances. Among the many structures reported in the literature, high SERS performances have been achieved by anisotropic particles with a central core and radial acute tips branching out, such as nanostars.[112–114] Another promising approach of fabricating nanoparticles supporting high SERS enhancements is incorporating internal hot-spots into a single particle. For instance, Mulvihill *et al.*[115] remodeled the structure of silver nanoparticles into highly anisotropic shapes with intraparticle gaps characterized by interesting optical properties and highly sensitive single-particle SERS response, *via* controlled anisotropic etching. Internal hot-spots were also generated in gold nanoparticles, such as for branched gold lace shells synthesized by Yang *et al.*[116] On the other hand, Lim *et al.*[117] designed gold nanobridged nanogap particles incorporating Raman reporter molecules in the 1 nm gap between the gold core and the gold shell which shows electromagnetic enhancements analogous to those observed at the gap of a dimer. Differently, Zhang and co-workers[106,107] developed core–shell nanoparticles displaying highly enhanced Raman signals from Raman dyes encapsulated in a dielectric core surrounded by a plasmonic shell.

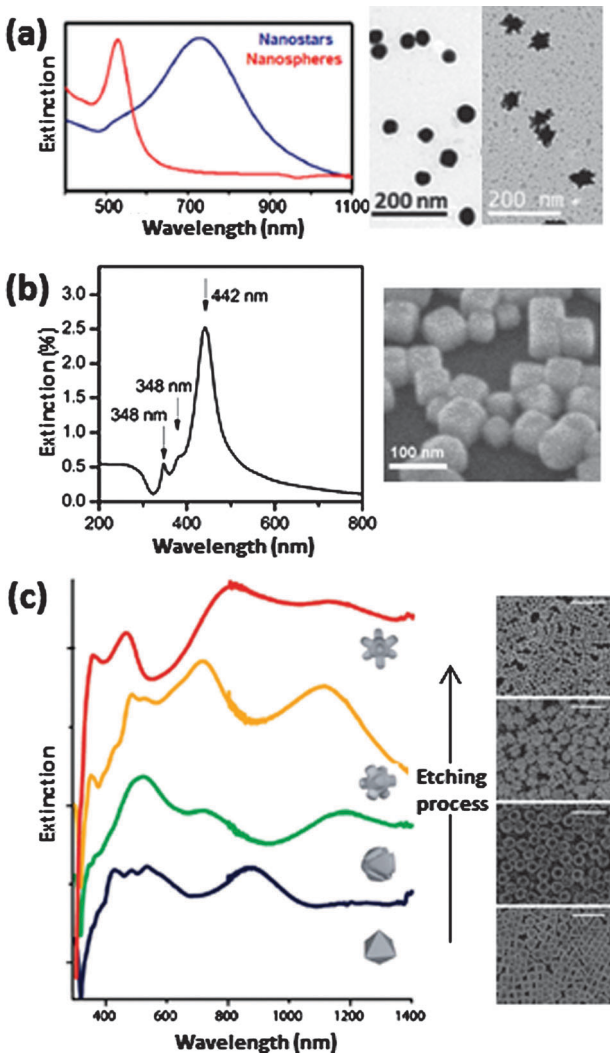

Fig. 4 Extinction spectra and TEM images of aqueous suspensions of: (a) gold nanospheres and gold nanostars (adapted with permission from ref. 102. Copyright 2010, American Chemical Society), (b) silver nanocubes (adapted with permission from ref. 217. Copyright 2011, American Chemical Society) and (c) silver octahedral-shaped particles (bottom structure) exposed to an etching process which progressively re-shapes the nanoparticle geometry. All scale bars shown represent 1 μm. Adapted with permission from ref. 115. Copyright 2010, American Chemical Society.

In general, the design of plasmonic nanoparticles with improved EM enhancing ability is of particular importance for expanding the potential of SERS substrates in imaging and sensing applications since it would overcome several of the intrinsic difficulties in fabricating highly SERS-active nanoparticles with reproducible and uniform response *via* assembly strategies.[118] Fig. 4 illustrates a few examples of anisotropic noble metal nanoparticles and their respective optical responses. For more details on shape-controlled synthesis and optical properties of these asymmetric nanoparticles, we refer the reader to several excellent reviews.[92,97,119] Major drawbacks for SERS applications of asymmetric nanoparticles are mostly related to their synthetic methods which usually require polymers, such as PVP, or surfactants, such as CTAB, as shape-directing agents. These chemicals normally remain firmly bound to the metal after the synthesis preventing the direct adsorption of a large number of potential analytes and often hampering the chemical functionalization of the surface unless extended and, critical for the nanoparticle stability, post-removal steps were performed.[38,96,120]

Plasmon coupling in interacting nanoparticles

An important additional feature of LSPRs, besides their dependence on shape, size and composition of the metal nanostructure and the surrounding dielectric environment, is observed when nanoparticles are in close proximity to each other: the plasmon coupling. In the simplest case of a dimer structure, the electromagnetic interaction between the two nanoparticles produces a drastic change of the extinction profile and the single LSPR of the isolated spheres (Fig. 5, black line) is split into two well-separated peaks (Fig. 5, red line), as similarly observed for gold nanorods (Fig. 3).

When the polarization of the incident light is perpendicular to the dimer axis, the plasmon coupling is minimal and the optical response of the dimer resembles that of the isolated object with only one slightly blue-shifted band in the extinction spectra (single-particle-like resonance, Fig. 5, blue line).[121,122] On the other hand, the plasmon coupling is maximized for incident polarization along the axis and two different contributions can be distinguished in the extinction spectrum (Fig. 5, green line): one weak feature at lower wavelengths prevalently associated with quadrupole modes and a second much more intense red-shifted plasmon band arising from the dipolar coupling of the individual LSPRs of the spheres. In the case of Au, single-particle-like and quadrupolar features are extremely weak or completely absent in the extinction spectrum of the gold dimer due to the strong damping of plasmonic resonances below $\sim$600 nm.[51]

The plasmon coupling of the interacting nanoparticles has a dramatic effect also on SERS, localizing large local fields at the

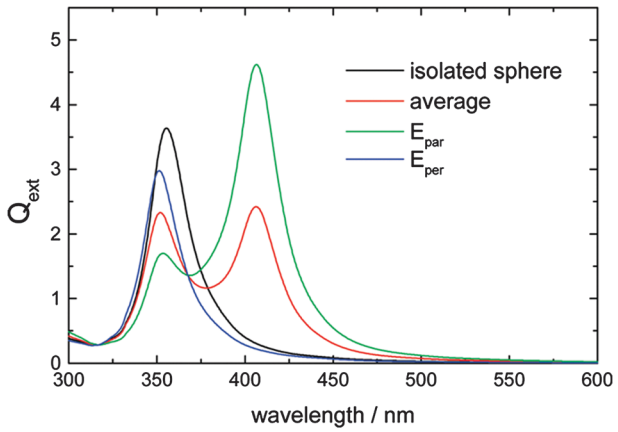

Fig. 5 Theoretical extinction spectra for parallel (E_{par}) and perpendicular (E_{per}) incident polarization with respect to the dimer axis on the extinction spectrum of a Ag dimer (diameter = 30 nm) in vacuum. The average extinction spectrum for both polarizations (red line) and the extinction spectrum for the single sphere (black line) are also shown. Reprinted with permission from ref. 122. Copyright 2010, American Chemical Society.

interparticle junction (also named "hot spot") that may exceed up to 10^3–10^4 times those observed on an isolated nanoparticle providing enhancement factors sufficient for single-molecule detection.[19] For a better understanding of the several effects that nanoparticle assembly has on the SERS properties and therefore practical applications of the colloidal system, it is worth recalling some fundamental aspects that describe the connection between the coupling of the localized surface plasmon resonances at the interparticle gap and the resulting SERS enhancements.

Among many types of nanoparticle assembly, dimers are arguably the simplest structure and can be considered as the building block of each cluster. For this reason, dimers are also widely used as a model to analyze and interpret more complex experimental results.[18,123] A large number of theoretical calculations describing the plasmonic and enhancing properties of dimers consisting of spherical Au and Ag nanoparticles of various sizes separated by different interparticle gaps can be found in the literature (for instance, see ref. 51, 121, and 123). As a representative example, we resume the most important aspects of the theoretical studies reported by Le Ru and Etchegoin in their book "*Principles of Surface-Enhanced Raman Spectroscopy*"[51] describing dimers formed by two identical spheres (radius a = 25 nm, either Ag or Au) immersed in water and illuminated by an incident source polarized along the dimer axis (*i.e.* maximum coupling of the LSPRs of each nanoparticle) (Fig. 6). In relation to SERS, the key findings of these studies are the following:

- The red-shifted resonances arising from plasmonic coupling of interacting nanoparticles (we refer to these contributions as gap-plasmon resonances) are typically the most important for SERS since they determine the dramatic EM enhancement at the hot spot.
- Gap-plasmon resonances and the local SERS EFs at the interparticle junction are highly sensitive to the interparticle distance, g: as the nanoparticles are pulled close together, the gap-plasmons are progressively red-shifted and the local SERS EFs at the hot-spot undergo a dramatic increase. However, these interparticle distance dependencies are rather different, in fact relatively large enhancements can be observed in spectral regions outside the main gap-plasmon resonance[123] (see for instance extinction and EF values for a 1 nm gap dimer at 800 nm). As a result, if a qualitative connection between the extinction profile and the SERS EFs for individual nanoparticles can be outlined, in the case of ensembles of interacting objects very little information can be extracted about the SERS EFs from the overall extinction spectrum.[123]
- As previously indicated for asymmetric-shaped nanoparticles, tuning the plasmon resonance in the near-infrared range is particularly important for Au nanostructures to overcome the strong plasmon damping observed below ~600 nm.

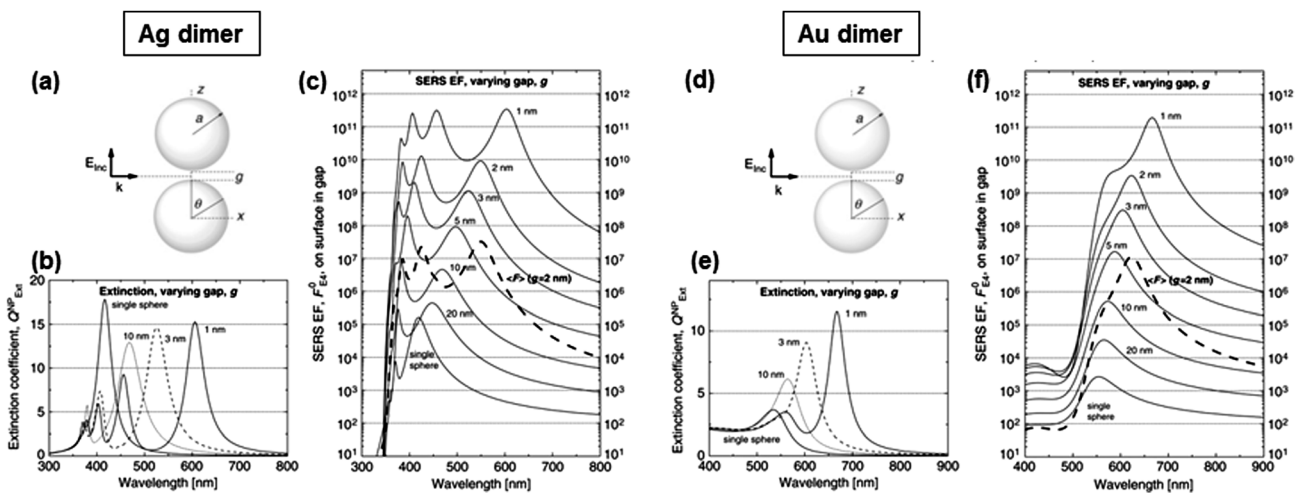

Fig. 6 (a, d) Schematic configuration of dimers formed by two Ag (a) or Au (d) spheres of radii a = 25 nm and separated by a gap g. The incoming wave is polarized along z (axis of the dimer) and with wave-vector k along x. (b, e) Extinction coefficients, Q_{ext}, for varying gaps as functions of incident wavelength for Ag (b) and Au (e) dimers. (c, f) SERS EF at the hot-spot for Ag (c) and Au (f) dimers. Also shown (thick dashed line) is the average SERS EF in the case of a g = 2 nm gap. Note that the resonances in the SERS EF have their counterparts in the extinction spectra, although their respective magnitudes are very different. Reprinted with permission from ref. 51. Copyright 2009, Elsevier.

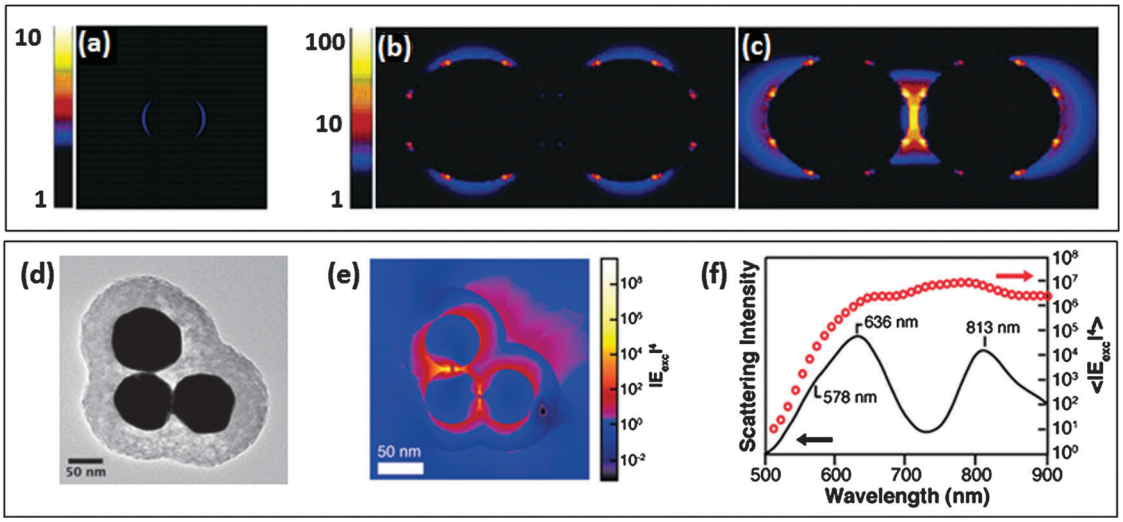

Fig. 7 Theoretical calculations of the local electromagnetic near field enhancement at the laser excitation wavelength of 632.8 nm for an isolated Au nanosphere of 30 nm radius (a), and an adjacent nanosphere dimer (interparticle distance 3 nm) with interparticle axis perpendicular (b) and parallel (c) to the incident polarization. The color scale represents the electromagnetic field enhancement $|E_{632.8nm}|$: (a) was calculated using Mie scattering theory, whereas (b) and (c) using the FDTD method. Adapted with permission from ref. 124. Copyright 2005, American Chemical Society. (d) TEM image of a Au trimer cluster encapsulated in a silica shell and (e) the corresponding image of the calculated electromagnetic enhancement intensity profile at 632.8 nm, $|E_{632.8nm}|^4$. The maximum and average EFs are 3.2×10^9 and 1.1×10^6, respectively. (f) Corresponding extinction spectrum of the Au trimer obtained by dark-field Rayleigh scattering microscopy and the calculated $|E_{exc}|^4$ as a function of the excitation wavelength (red open circles). Adapted with permission from ref. 125. Copyright 2010, American Chemical Society.

In fact, for isolated spherical nanoparticles, the maximum SERS EFs of Ag exceed that of Au by $\sim$2 orders of magnitude whereas for highly interacting objects (1 nm gap) the local EFs at the gaps are similar.

• The decrease of the interparticle distance in the dimer leads to stronger local enhancements but with an increasing degree of spatial localization (*i.e.* higher local EFs extend over a smaller volume around the hot-spot). This has two immediate consequences:

(i) The difference between the local EF at the gap and the average SERS EF obtained by averaging the different contributions of a dimer randomly oriented with respect to the incident light polarization (dashed line, for interparticle distance = 2 nm) is higher for shorter interparticle distances. For a general idea, typical highly interacting nanoparticles in partially salt-aggregated Ag colloids show the AS-EF/SM-EF ratio $\sim 10^{-4}$.[109] The SERS efficiency of the assembled system can be potentially improved to $\sim 10^{-3}$ for a monodispersed dimer suspension and further more in the case of specific analyte adsorption at the hot spot.[109]

(ii) The difference diffusion and/or positioning of molecules in the hot-spot volume may become a difficult factor to control in the SERS experiments for very short gaps. As a general rule for SERS substrates, the reproducibility and uniformity of the enhancement across the nanostructure are improved to the detriment of the maximum SERS activity.

In order to provide a simple physical visualization of the aspects of the plasmonic coupling in interacting nanoparticles discussed in this section, we report two examples of theoretical simulations of local field enhancements in a gold nanoparticle dimer and trimer. Fig. 7a–c illustrates the finite difference time domain (FDTD) calculations at the excitation laser wavelength of 633 nm performed by Talley *et al.*[124] for an isolated Au nanosphere (30 nm radius, Fig. 7a) and the corresponding homo-dimer (3 nm gap distance) both for polarizations along and perpendicular to the interparticle axis (Fig. 7b and c, respectively). This figure explicitly shows the high degree of spatial localization of the local field enhancements at the interparticle junctions, together with its strong dependence on the laser polarization. Additionally, Fig. 7 shows the TEM image of a Au trimer encapsulated in a silica shell (Fig. 7d) and the corresponding profile of the electromagnetic enhancement at 633 nm (Fig. 7e) with the extinction spectrum.[125] The two nanoparticles at the bottom of the trimer structure appear to be coalesced where the distance between the two vertically oriented spheres was estimated to be <1 nm. The calculated average field enhancement illustrated in Fig. 7f (red open circles) shows a nearly wavelength independent nature demonstrating the poor or null connection between SERS EFs and the plasmon profile in the case of interacting nanoparticles.[125]

Assembly strategies of colloidal nanoparticles

The colloidal suspension is a metastable system, whose stability is determined by a balance between the long-range Van der Waals attractions and short-range electrostatic repulsions of the double-layer of counterions surrounding the nanoparticles (metallic colloids are usually charged). The combination of these two opposite effects is at the core of the Derjaguin, Landau, Verwey and Overbeek theory (DLVO),[126] which describes the nanoparticle stability in a colloidal system. Other factors not included in this theory, such as steric hindrance and hydrodynamic forces (interaction though movement in the fluid), may play in reality an important role in the overall equilibrium of the colloid.

The simplest way to induce nanoparticle aggregation is based on increasing the ionic strength by the addition of an electrolyte to the colloid which decreases the Coulombic repulsions that ensure the nanoparticle stability. It is possible to recognize different classes of aggregating agents on the basis of different degrees of modifications that may be introduced into the colloidal system.[51] For instance, salts such as KNO_3 and $MgSO_4$ (passive electrolytes) merely increase the ionic concentration without firmly binding the metal surface,[127] whereas active electrolytes (such as halide salts NaCl and KBr) lead also to substantial modification of the nanoparticle surface chemistry *via* strong halide–metal interactions,[128] especially in the case of Ag.[120,129]

A further aggregation strategy is to introduce charged molecules or polymers which act as electrostatic bridges between the nanoparticles. For most common colloids, the nanoparticle surface at the metal–liquid interface is negatively charged due to the presence of anions such as citrate,[130] chloride[131] and EDTA[132] as capping agents. Therefore, nanoparticle aggregation can be mediated by addition of the positively charged molecules such as spermine[133] and poly(L-lysine).[134] For all these different approaches to promote particle aggregation and thus the formation of hot spots, it would be desirable to have a stable colloidal system, at least on the experimental time scale, in order to avoid significantly time-dependent and irreproducible results.[51]

Randomly aggregated large nanoparticle ensembles have been shown to provide huge SERS enhancement which enabled the detection of single molecules using SERS (SM-SERS).[20,21] However uncontrolled nanoparticle assemblies, even from highly monodisperse systems, inherently suffer from poor uniformity in terms of interparticle spacing, geometry and numbers of particles per cluster. For SERS measurements carried out by investigating a relatively large volume of colloidal clusters, these structural inhomogeneities can be smoothed by creating stable fully aggregated colloids,[135] in order to avoid time-dependent results.

Nonetheless, for most practical applications the ideal SERS platform would be that of a stable dispersion of small colloidal clusters with well-defined geometrical properties and controlled hot spot architecture providing simultaneously high SERS activity and signal reproducibility. In an attempt to address this issue, various strategies have been reported in the literature to control the organization of nanoparticles in suspension to generate efficient SERS substrates, which can be broadly summarized as follows:

(1) Control of the aggregation kinetics by optimizing the aggregating salt concentration in order to maximize the formation of dimers/trimers and reduce the yield of larger aggregates.

(2) Use of molecular nanoparticle cross-linkers to engineer interparticle junctions in a controllable manner.

Once more, we have to underline that the design of the nanoparticle assembly in terms of EM enhancement, stability, accessibility to the interparticle junctions by external analytes, reversibility, post-treatment processes, *etc*. is dictated by the specific application envisaged by the experimentalist.

All the works discussed in the following section deal with the nanoparticle assembly in suspension. The corresponding SERS measurements are similarly performed by the authors in the dispersed phase, unless when specified.

Aggregating agents: controlling the aggregation kinetics

Meyer *et al*.[136] demonstrated that, by careful control of the level of the KCl salt added to silver citrate colloid, it is possible to achieve a metastable aggregation state with limited Coulomb-blocked aggregation at the onset of instability in a colloidal dispersion. In this situation the Coulombic barrier still exists to prevent extended coagulation of the colloid but is not large enough to ensure a long-lived monodispersed state of individual nanoparticles, determining a self-limiting aggregation dynamics that results in the formation of metastable dimers, trimers and small clusters in suspension. This approach has been also utilized for SM-SERS using a bi-analyte strategy after a proper dilution of the colloid, to ensure that only one small aggregate resides in the laser probe volume under investigation.[137,138] Li *et al*.[139] described a one-step method to generate Ag nanosphere dimers with $\sim$1.8 nm gap in good yields ($>50\%$) by optimizing the amount of chloride anions added to a nanoparticle polyol synthesis to control both colloidal stability and oxidative etching. Similarly, the same authors also developed a simple method to produce dimers of Ag nanospheres based upon wet etching with $Fe(NO_3)_3$ from Ag nanocubes in ethanol and in the presence of PVP.[140] However, even at low concentration the use of active electrolytes, such as chloride salts, may lead to significant modifications of the NP surface chemistry, limiting in some cases the adsorption of analytes and their SERS detection. In this regard, Larmour *et al*.[141] replaced chloride salts with a passive electrolyte such as $MgSO_4$ in the self-limited aggregation of silver citrate nanoparticles into dimer-enriched suspensions. These small clusters retain their original weakly bound citrate surface layer, easily displaceable by a much broader spectrum of molecules.

Controlled synthesis of small nanoparticle clusters can be followed by a successive encapsulation of the aggregates within polymer shells[142,143] or silica coating.[144,145] This post-treatment stabilizes the ensembles preventing, on the one hand, unwanted dissociation or further aggregation and, on the other hand, allowing purification and isolation of large quantities of dimers and trimers *via* post-centrifugations. Achieving high homogeneity of SERS enhancements over individual clusters is a key factor for their application in quantitative measurements, either *via* an intrinsic or extrinsic strategy. However, when an impermeable barrier surrounds the nanostructures, the adsorption of analytes on the metal surface is completely hindered in most of the cases and the exploitation of these nanoparticle assemblies is limited to extrinsic SERS applications where a Raman reporter molecule is allowed to diffuse into the hot spots prior to the shell coating (encoding process). The external silica or polymer shell of SERS-encoded clusters can then be functionalized with chemical or biological recognition elements to selectively target specific analytes.

Major limitations to the application of extensive use of nanoparticle clusters obtained *via* careful control of the electrolyte concentration as SERS substrates are the limited control over the interparticle distance, which markedly affects

the homogeneity of the SERS enhancement at each individual aggregate, and the restricted accessibility to the hot-spot that analytes may experience, especially for relatively large molecules, for short gaps as those generated in salt-aggregated colloid.

Self-assembly mediated by molecular linkers

The use of molecules as nanoparticle cross-linkers has been shown to be a more efficient strategy to control and design the interparticle properties and the geometrical structure of Ag and Au clusters. It is possible to generally classify the molecular linkers into two major categories (Fig. 8):

(1) Bifunctional molecules

Linkers contain functional groups usually placed at opposite ends of the molecular structures, such as dithiol- or diamine-containing linkers, which bind the metal surface *via* covalent bonds or electrostatic interactions.

(2) Molecules with selective recognition ability

In this strategic scheme, nanoparticle surfaces are usually modified with molecules which promote the assembly in response to external stimuli such as the presence of the target analyte, changes in pH or upon UV irradiation. This is the case for instance of complementary DNA strands attached to nanoparticle surfaces that undergo selective hybridization promoting the reversible formation of clusters.

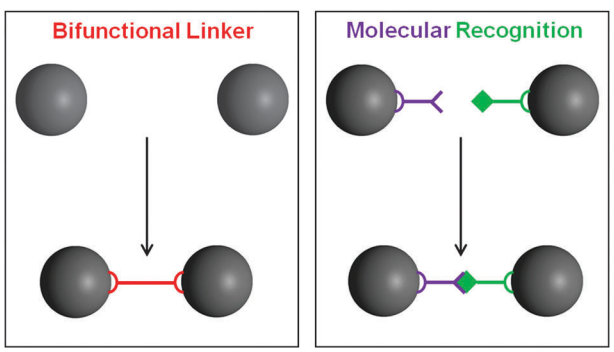

Fig. 8 Schematic description of the two main different classes of molecular linkers employed to assemble colloidal nanoparticles in suspension.

Non-biological linkers. Extensive research on the use of bifunctional molecules to engineer hot-spots into SERS active nanostructures was pioneered by Moskovits and co-workers who successfully employed various classes of linkers such as dithiol-[146–148] and diamine-containing molecules.[149]

Vlckova *et al.*[149] investigated single-molecule SERS at individual hot-spots of silver dimers formed by assembly of small clusters using 4,4′-diaminoazobenzene as a bifunctional linker with high Raman cross-section (Fig. 9). Approximately 1 to 1 linker-to-nanoparticle ratio was selected to both limit the distribution of aggregates to very small ones dominated by dimers and statistically locate a single bifunctional molecule at the hot spot. SERS spectra collected on a single dimer level after chemical deposition on TEM finder grids showed temporal fluctuations (blinking) with long recurrence times likely associated with single-molecule dynamics (Fig. 9).

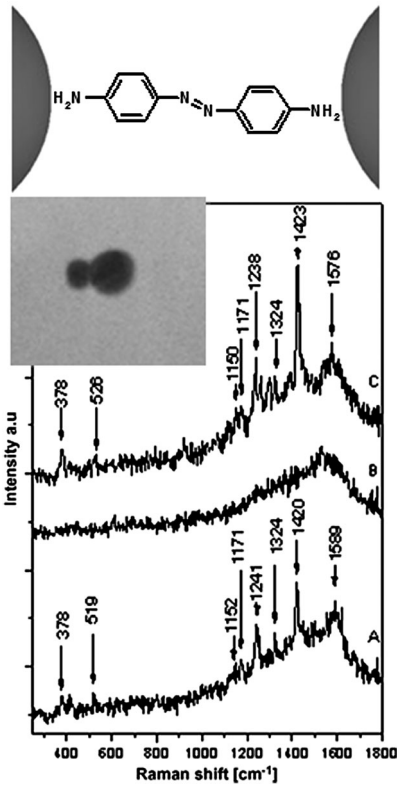

Fig. 9 TEM image of a selected Ag nanoparticle dimer linked by 4′-diaminoazobenzene (see the top scheme for the linker molecular structure) and SERS signals obtained at different times by investigating the same dimer cast over the grid. Adapted with permission from ref. 149. Copyright 2008, Elsevier.

Bifunctional molecules combining nanoparticle-bridging ability with high Raman cross-sections are particularly favored in the fabrication of SERS-encoded clusters for extrinsic applications. In this regard, Fabris and co-workers reported high yield synthesis of Ag dimers in suspension *via* controlled aggregation using distyrylbenzene[150] or 4,4′-dimercaptobiphenyl.[151] Subsequent functionalization of 4,4′-dimercaptobiphenyl-linked Ag dimers with aptamer sequences was carried out to impart selective recognition properties and their application as an effective SERS-encoded substrate for protein detection. The design of the heterogeneous assay is outlined in Fig. 10 and it has been reported here to provide to the reader a common example of application of SERS-encoded clusters to analytical problems.

Braun *et al.*[148] extended this strategy to engineering inter-particle junctions *via* dithiol linkers by combining it with a microsphere patterning technique to fabricate SERS substrates where the position of the hot spots can be easily localized by common optical microscopy. Surfaces of silica microspheres (Fig. 11) partially modified with amino groups were used to bind Ag nanoparticles and concentrate them at specific points on the microsphere. Bifunctional dithiol linkers such as 1,4-benzenedithiol or OPV (thioacetyl-terminated oligo phenylenevinylene) were then used to link Ag nanoparticles/microspheres together. Once assembled, the microaggregates were deposited on TEM grids where the interparticle area containing the hot spots could be easily located by optical

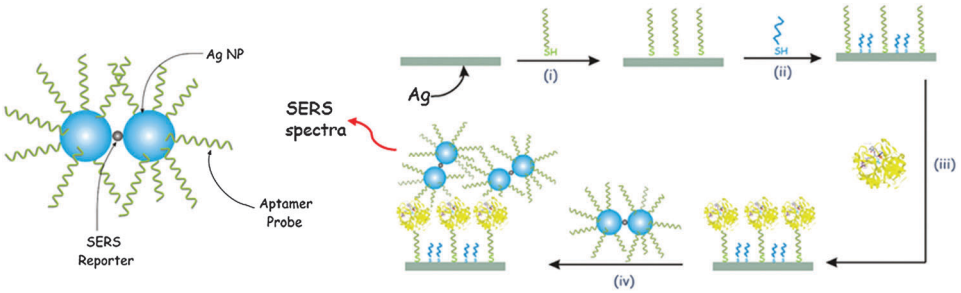

Fig. 10 Schematic representation of the SERS-encoded Ag dimer functionalized with aptamer probes (left drawing) and its application to the detection of thrombin. The heterogeneous assay is composed of the following steps: (i) functionalization of a silver layer deposited over a silicon wafer with protein-specific aptamers; (ii) residual uncoated surface area is covered with mercaptohexadecanoic acid to prevent unspecific protein adsorption; (iii) target thrombin molecules are bound by the aptamer whereas physically adsorbed proteins are selectively washed away; (iv) aptamers-SERS-encoded dimers bind to the protein *via* a second recognition site. The characteristic SERS spectra of the Raman reporter inform about the presence of the thrombin. Adapted with permission from ref. 151. Copyright 2008, John Wiley and Sons, Ltd.

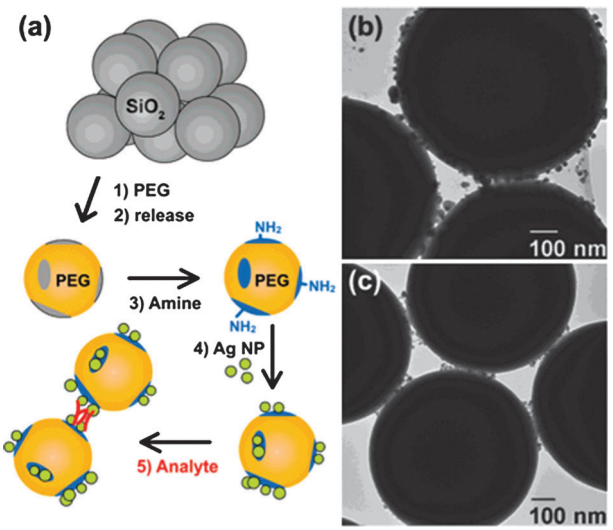

Fig. 11 (a) Schematic of the five-step process for molecular-linker controlled nanoparticle-patterned microsphere (MS) assembly: (1) silica MSs are centrifuged to form a close-packed network. The exposed surface silanols are functionalized with PEG-silane before (2) being redispersed. (3) Residual surface silanols groups are functionalized with aminosilane in order to (4) selectively bind Ag nanoparticles. (5) Dithiol molecules are added, leading to crosslinking. (b) and (c) TEM images of Ag nanoparticles/MSs, cross-linked by OPV: (b) unmasked MSs functionalized with aminosilane and (c) contact masked MSs patterned first with PEG-silane and then with aminosilane. Reprinted with permission from ref. 148. Copyright 2007, American Chemical Society.

microscopy and the SERS response investigated at the single cluster level. However, the self-assembly of nanoparticles *via* strongly adsorbed linkers limits the SERS application of these structures for intrinsic SERS detection purposes since the bridging molecules tend to stop the diffusion of the analyte at the interparticle junction. In order to overcome this limitation, the authors described in a subsequent study[152] the use of 1,6-diaminohexane as a sacrificial linker. This diamine can easily be displaced at a later stage from the interparticle gap by subsequent infusion of small analytes with higher affinity toward the metal surface. In this article, they reported a general kinetically optimized linking protocol to assemble colloidal silver nanoparticles into polymer-encapsulated dimers and small clusters in high yields, showing a high and reproducible SERS response.[153] Assembly of nanoparticles was also achieved by using different thiol-containing reporters providing intense SERS spectra (Fig. 12). The aggregation kinetics was optimized to maximize the formation of dimers and small clusters and followed by a polymer addition step (PVP and thiol-PEG) which both stops further aggregation events and stabilizes the clusters. The highly bulky nature of the selected polymer molecules avoids their access to the narrow interparticle region, providing a stabilizing external shell which is relatively permeable for the diffusion of

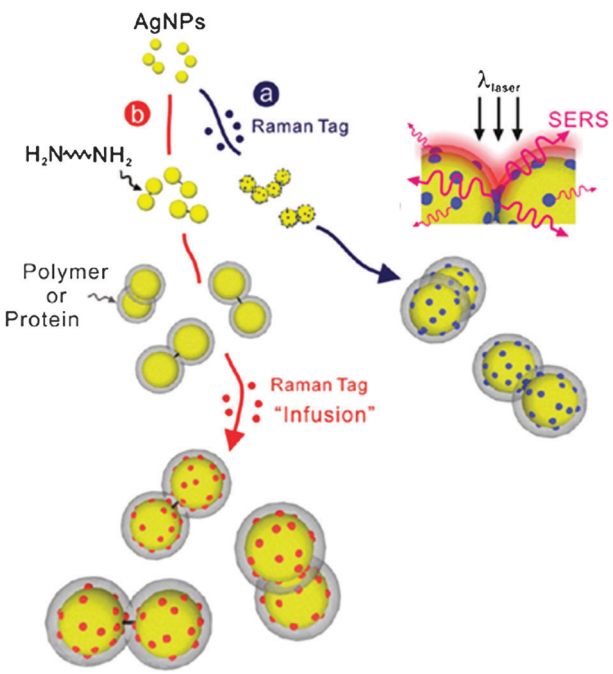

Fig. 12 SERS nanocapsule synthesis. (a) Ag nanoparticles are cross-linked with the bifunctional linker 4-aminobenzenethiol (ABT, blue) or (b) 1,6-hexamethylenediamine (HMD, black), and then coated with a layer of PVPA. PEG-thiol or streptavidin and bovine serum albumin proteins are then adsorbed (not shown). In (b), the SERS tag (red) is infused through the polymer coat. Adapted with permission from ref. 152. Copyright 2009, American Chemical Society.

small analytes. Guerrini *et al.*[154] demonstrated that, by varying the length of the alkyl chain, the interparticle distance of the diamine-linked nanoparticles can be finely tuned in the $\leq$2 nm range.

As for any other intrinsic SERS detection of target analytes, chemical functionalization of the substrate is often required to impart higher selectivity and sensitivity, especially in the case of molecules with little or no affinity toward the metal surface. In the case of engineered NP clusters, the diffusion of the target species at the hot spot is a key factor for maximizing the analytical sensitivity. In this regard, Sanchez-Cortes and co-workers[81,155,156] explored several approaches for the ultrasensitive detection of polycyclic aromatic hydrocarbons (PAHs), by concentrating these pollutants with low affinity for the metal surface at the interparticle gaps of silver clusters assembled *via* molecular linkers which act also as hosts for PAHs. In the first strategy (Fig. 13a), the assembly of silver nanoparticles was mediated by the bifunctional viologen dication, Lucigenin, which contains two aromatic ring moieties free to rotate around the C–C inter-ring bond leaving room for hydrophobic intermolecular cavities at the metal surface with high affinity for PAH molecules.[155,156] SERS detection of a few molecules (zeptomole range) of 'non-SERS-active' PAHs, such as pyrene, has been reported by the authors. Alternatively, calixarene dithiocarbamate-derivatives were employed to promote the capture of PAHs at the metal surface.[81,157,158] In this case, the calixarene host simply acts as a molecular host and the hot spot formation is only triggered when the PAH analyte possesses the appropriate size to induce a dimeric encapsulation driven by the π–π

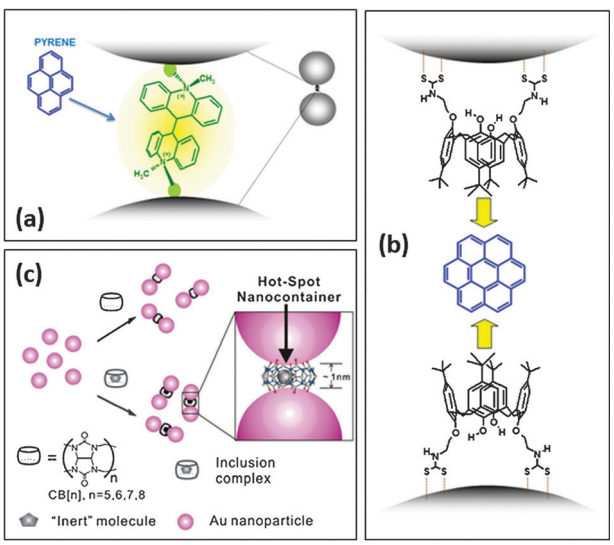

Fig. 13 Schematic illustrations of: (a) architecture of the interparticle junctions mediated by the Lucigenin linker and the approaching of the target PAH molecule (pyrene) at the gap. Adapted with permission from ref. 156. Copyright 2009, American Chemical Society. (b) Formation of nanoparticle bridges by dimeric complexation of calixarene hosts with coronene PAH. Adapted with permission from ref. 81. Copyright 2009, American Chemical Society. (c) Fabrication of the SERS hot spot nanocontainer system through bridging Au nanoparticles using CB[*n*] macrocyclic compounds. Reproduced from ref. 84 with permission from The Royal Society of Chemistry.

interaction between the host and guest aromatic rings (Fig. 13b). Recently, Tao *et al.*[84] used cucurbit[*n*]uril 'nanocontainers' as bifunctional linkers to control the interparticle gap formation in gold nanoparticle assemblies (Fig. 13c). In this case, the inclusion binding ability of the host cucurbit[*n*]uril was exploited to first selectively encapsulate analytes with poor affinity toward the metal surface and then to induce the formation of well-defined nanogaps at small gold nanoparticle clusters locating the target molecule exactly at the hot spot.

Engineering the interparticle gap with controlled geometrical properties in a gold nanoparticle assembly was also investigated by Yan *et al.*[159] using methylthio arylethynes with different shapes and functional groups as rigid binfunctional linkers providing intense SERS features.

Interparticle junction formation in colloidal systems specifically designed to be mediated by the presence of the target analyte has also been employed for instance in the ultra-trace detection of metal ions such as Ni(II),[90] as shown in Fig. 2, and explosives such as TNT.[160]

pH-responsive SERS assemblies consisting of specifically functionalized nanoparticles whose aggregation is selectively switched on/off by changes in aqueous pH were reported in the literature. For instance, Qian *et al.*[161] designed gold nanoparticles modified with thiolated block copolymers consisting of a polymethacrylic acid (PMAA) block, an amphiphilic polyethylene glycol (PEG) block, and a terminal lipoic acid anchoring group (Fig. 14a). At pH $<$ 4, the PMAA segment undergoes a reversible conformational change from an expanded structure to a collapsed conformation. In the case of the polymer-coated nanoparticles (Fig. 14b), this structural reorganization at acidic pH leads to a drastic shortening of the interparticle distance and, in turn, a large increase of the electromagnetic enhancement at the gap, as revealed by the appearance of an intense SERS signal from the Raman reporter molecules located at the metal surface (Fig. 14c). In a separate study, Taladriz-Blanco *et al.*[162] modified gold and silver nanoparticles with DL-penicillamine and *N*-acetyl-DL-penicillamine to control the reversible nanoparticle aggregation. At acidic pH, the protonation of the penicillamine carboxylic groups promotes the formation of intermolecular hydrogen bonds and thus the nanoparticle assembly.

As previously mentioned, spherical or spherical-like Ag and Au nanoparticles synthesized *via* a common reduction reaction in aqueous solution (for instance, citrate-reduced colloids) are widely used as building blocks for controlled assembly since their aggregates are an effective source of intense SERS enhancement and because their relatively 'naked' surfaces are readily available for chemical functionalization. Nonetheless, expanding the use of anisotropic nanoparticles with different shape and composition as building blocks for controlled assembly would provide an extremely powerful tool to engineer nanostructures with a much wider spectrum of plasmonic properties.[163,164] However, the development of controlled assembly strategies for anisotropic building blocks is still at its infancy and remains a great challenge. Particular efforts have been devoted to the rational assembly of gold nanorods (GNRs)[165] through many different strategies. For instance, Zhong *et al.*[166] exploited the different surface properties of

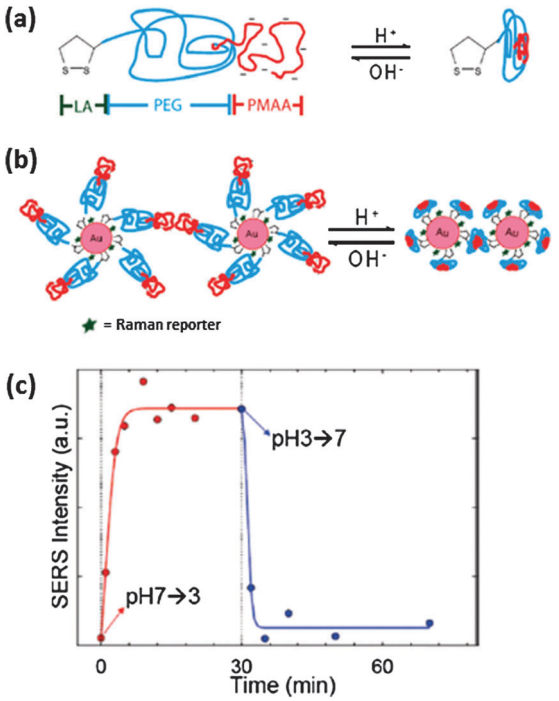

Fig. 14 Schematic of the (a) molecular structure and pH-induced conformational changes of the thiolated two-block copolymer formed by a pH-responsive polymethacrylic acid (PMAA), an amphiphilic polyethylene glycol (PEG) block, and a terminal lipoic acid anchoring group. (b) Shortening of the interparticle distance in nanoparticle assembly induced by polymer conformational changes. (c) Time-dependent evolution of the SERS intensity of the Raman reporter band at 1498 cm^{-1} between pH 7 and 3. Adapted with permission from ref. 161. Copyright 2009, American Chemical Society.

GNRs to selectively introduce thiol-PEG and thiol-PEG-COOH ligands either at the tip (100 face) or at the side (110 face) of the rod promoting the controlled assembly of GNRs in a side-by-side, end-to-end or end-to-side fashion *via* electrostatic interaction between the positively charged CTA^+ and the carboxylate group COO^-, whereas HS-PEG acts as a blocking agent. As expected, end-to-end assembly with interparticle gaps formed by bridged nanorod tips provided higher SERS enhancements as compared to end-to-side and side-to side organization. Alternatively, external anion molecules such as EDTA[167] or sodium citrate[168] have been employed to mediate the electrostatic assembly of GNRs in a reversible manner or to obtain dimers and trimers in high yields, respectively, with improved SERS responses. However, the SERS enhancement gained when assembling GNRs is partially hampered by the CTAB layer thickness,[45] which limits the tuning of the interparticle distances approximately in the >5 nm range.

Chen *et al.*[169] employed GNRs assembly to investigate the effect of the physical stress that high local electromagnetic fields at the hot spot may exercise on the adsorbed molecule and, in turn, on its SERS spectrum. Anisotropic polymeric encapsulation of GNRs at the side of the nanostructure limited the adsorption of the Raman reporter (4-MBA) at the tip ends and promoted linear aggregation of the particles. In this way, the SERS response of the colloidal assembly was uniquely provided by those molecules localized at the hot spots, avoiding averaging effects observed for randomly aggregated spherical gold nanoparticles, and highlighted dramatic alteration of the SERS fingerprint resulting from molecular reorientation at the hot spot. For a state-of-art overview of different self-assembly strategies of GNRs and their applications, the reader may refer to ref. 165.

Biological linkers. Biomolecules, such as antibodies and antigens, proteins and DNA, have also been successfully exploited to assemble metallic nanoparticles. In particular, DNA represents one of the most outstanding materials for bottom-up engineering of rationally designed plasmonic nanoparticle assembly thanks to its extraordinary properties,[3,49,170] such as molecular recognition, structural plasticity and programming capabilities to precisely direct the nanoparticle organization into an impressive variety of complex morphologies,[3,72,171–180] including post-assembly reconfiguration of the plasmonic nanostructures *via* molecular stimuli.[181]

Reversible aggregation of oligonucleotide-functionalized nanoparticles containing a Raman reporter by ssDNA hybridization to manipulate SERS signals was pioneered by Graham and co-workers[177] followed by Nie and co-workers.[182] In these studies, silver[177] and gold nanoparticles[182] were functionalized with DNA probes and labeled with dye molecules as Raman reporters (Fig. 15). Addition of a target complementary to the two probe sequences results in the sequence-specific DNA hybridization which, in turn, determines extended nanoparticle aggregation and the consequent increase of the SERS signal. Subsequent heating of the colloidal system promotes the cluster disassembly through denaturation of the DNA duplex, and the corresponding disappearance of the additional SERS enhancement attributed to the interparticle junction formation. Appropriate selection of the excitation wavelength is critical for maximizing the SERS intensity ratio between the assembled and the monodispersed state.

This strategy was extended to the use of SERS to discriminate single base mismatching[183] and mutations in DNA sequences,[184] to several different ultra-sensitive DNA detections[185–196] and to the study of protein–DNA interactions.[197,198]

Recently, DNA in its natural state (double stranded, dsDNA) has been employed as a new promising approach to assemble gold nanoparticles conjugated with triplex-forming oligonucleotides for bio-applications.[195,199–201] As a molecular linker, dsDNA offers high structural rigidity overcoming flexibility and bending properties that limit the use of ssDNA when a strict control of the interparticle distance is required.[49,172]

Possibly, the major drawback of DNA as an assembling mediator for colloidal nanoparticles in SERS applications is the intrinsic limited ability of tuning interparticle gaps at short distances due to the length of the oligonucleotide sequences. In fact, sequences of at least 12 bases are usually employed to ensure stable conjugation to the target of interest and at least 15 bases to avoid nonspecific hybridization.[183] As a result, moderate enhancements can be generated at the junctions, which therefore are more appropriately addressed as a "warm spot" rather that hot spot.[202] Chen *et al.*[202] showed that the

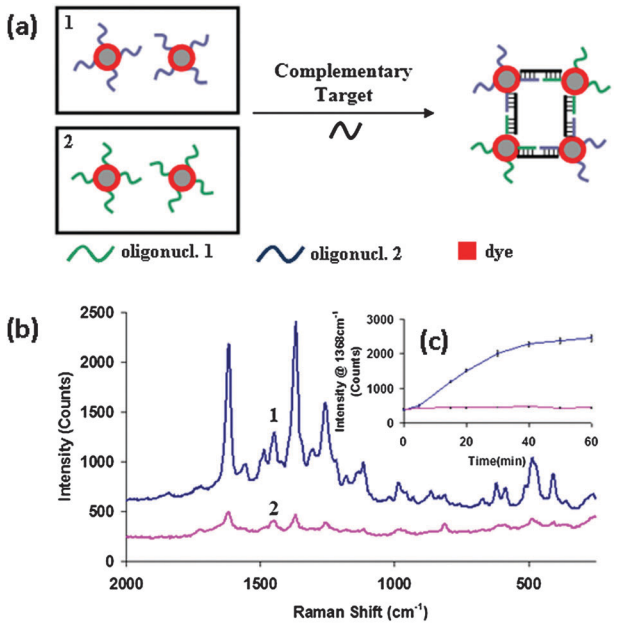

Fig. 15 (a) Schematic representation of single stranded DNA-driven assembly of Raman dye-functionalized oligonucleotide silver nanoparticle conjugates. Upon addition of a target single stranded DNA complementary to both sequences 1 and 2 on Ag nanoparticles, hybridization of the sequences occurs and results in aggregation of the nanoparticles. (b) SERS spectra of DNA-functionalized Raman dye-coded silver nanoparticles after being exposed to either a fully complementary target (1) or half complementary target (2) for 60 min. (c) Change in intensity at 1368 cm^{-1} over time. Adapted with permission from Macmillan Publishers Ltd: [Nature Nanotechnology] (ref. 177), copyright (2008).

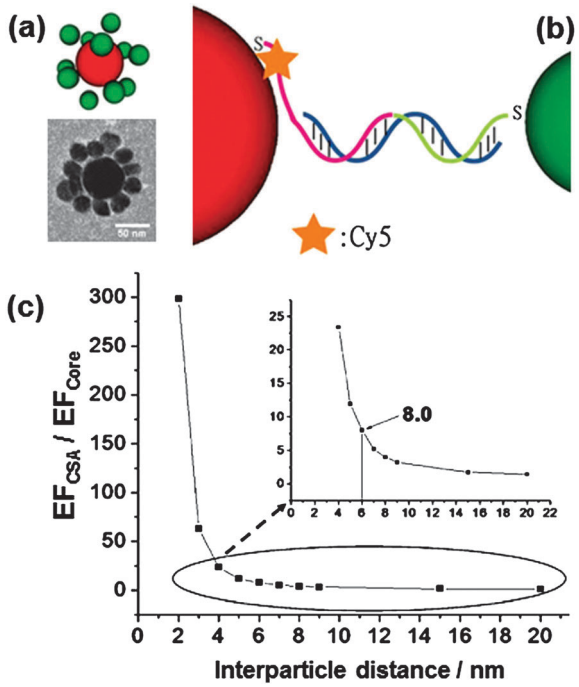

Fig. 16 (a, b) Representations of core-satellite assemblies (CSA) and TEM images of a CSA. (c) Ratio of core surface-averaged electromagnetic enhancement (simulated) for core particles in CSAs relative to isolated core particles as a function of separation between satellite particles and cores. The experimentally observed Raman scattering from Cy5 in the investigated coupled assemblies is amplified by a factor of 8.0. Adapted with permission from ref. 202. Copyright 2009, American Chemical Society.

nanoparticle separation imposed by the intrinsic DNA sequence length lies in the distance range providing moderate but more reproducible SERS enhancements. The authors investigated the SERS properties of core-satellite structures of gold nanoparticles (CSA) assembled *via* DNA molecular recognition, using an oligonucleotide strand incorporating a NIR-dye reporter, as outlined in Fig. 16a and b. The corresponding SERS intensity increase (Fig. 16c, expressed as the average enhancement ratio EF_{CSA}/EF_{Core}) produced by the nanoparticle aggregation is modest but, on the other hand, less susceptible to small changes of interparticle separations as compared to much narrower gaps, providing SERS substrates with quantitatively predictable enhancements.

Nonetheless, the intrinsic length of DNA poses a severe limitation to its use in the fabrication of highly SERS-active nanoparticle architectures for ultrasensitive applications. However, recent efforts have focused on strategies to overcome the limited interparticle spacing control provided by DNA molecular linking. Wang *et al.*[192] employed short locked nucleic acids (LNAs) with 7 bases to assemble nanoparticles *via* DNA hybridization into clusters with 2–3 nm gaps, taking advantage of the improved salt and thermal stability of the LNA-modified sequences.[195,203,204] On the other hand, Lim *et al.*[72] reported a novel strategy to synthesize highly effective SERS-encoded dimeric structures in high yields exploiting the DNA's ability to organize nanoparticle assembly with well-defined and reproducible hot spot properties. Fig. 17 outlines the fabrication method. Au nanoparticles of different size (20 nm diameter, probe A; and 30 nm, probe B) were functionalized with a combination of two DNA sequences, a protecting strand and a target-capture oligomer, under stoichiometric ratio to statistically introduce ~1 target-capture DNA per probe. In the case of probe B, a Cy3 dye was introduced in the target-capture sequence. Next, a magnetic-particle based separation method was performed to eliminate the fraction of probes without target-capture DNA strands prior to the heterodimeric assembly *via* DNA hybridization upon addition of the complementary target sequence. Importantly, a single Raman reporter molecule is placed exactly in between the two units of the heterodimer. Finally, controlled coating of the structures with silver shells generated interparticle gaps tuned at the nanometer scale down to the almost touching regime. The dimeric structure, spin-coated on a glass surface, provided single-molecule SERS detection sensitivity.

DNA-functionalization of plasmonic nanoparticles was also designed to fabricate pH-responsive SERS switching substrates in an aqueous environment.[205] Under acidic pH, the DNA conformation rearranges from a single stranded random coil structure to a compact folded conformation *via* half protonation of cytosine bases, promoting the reversible nanoparticle aggregation and the turn 'on' of the SERS signal.

Wang *et al.*[197] designed asymmetric assembly of spherical gold nanoparticles and gold nanorods, respectively, functionalized with a thrombin-binding aptamer and an anti-thrombin antibody

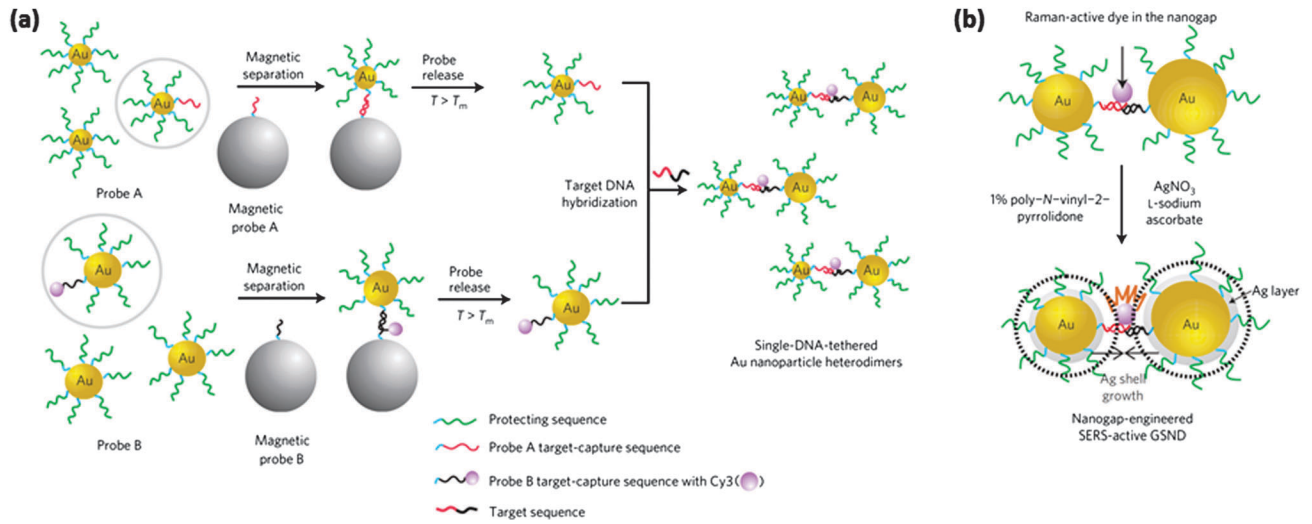

Fig. 17 (a) Synthetic scheme for the Au nanoparticle heterodimers using stoichiometric DNA modification and magnetic purification. (b) Nanometre-scale silver-shell growth-based gap-engineering in the formation of the SERS-active gold–silver core–shell nanodumbbells (GSND). Adapted with permission from Macmillan Publishers Ltd: [Nature Materials] (ref. 72), copyright (2009).

for the subnanomolar SERS detection of thrombin in human blood serum.

Label-free protein SERS detection near the single-molecule level was achieved by Pavel *et al.*[206] for two mutants of a small protein containing cysteine groups at axially opposite sides of the biomolecule. Upon reduction, the disulfide bonds were broken and the thiolate groups free to interact with silver nanoparticles forming interparticle hot spots.

Unraveling the correlation between SERS and extinction properties in large nanoparticle assemblies

As previously discussed in Fig. 3, a connection between the extinction profile and the SERS EFs for individual nanoparticles can be outlined, but fails when plasmon coupling between interacting nanoparticles occurs due to the different spatial localization of the plasmon resonances and the SERS enhancements that may result.[123] This is particularly evident in colloidal suspension as the clusters geometry become more and more complex, and short interparticle gaps with very large enhancements are present.[123]

In this regard, very recent efforts have been made to tackle the challenge of unraveling the relationship between geometrical features, plasmon properties and SERS enhancements in nanoparticle assemblies in suspension. This knowledge would provide crucial tools to predict, and design, the properties of the self-assembled system in a reproducible manner pushing the application of these structures to a wider range of sensing and nanophotonic devices.

Most of these studies were carried out at the single cluster level.[73,139,207,208] Wustholz *et al.*[125] investigated structural and optical properties of 30 individual small clusters of gold nanoparticles coated with a monolayer of Raman reporter and "frozen" in their configuration by encapsulation in a silica shell to guarantee uniform distribution of the analyte at the hot spots and preserve structural stability. They observed that the average SERS EFs of small clusters, cast over a TEM grid, are largely determined by the contribution yielded by the shorter interparticle gap, and addition of further nanoparticles to the dimer structure does not afford significant increase to the overall SERS enhancement. Using a similar nanofabrication strategy, Chen *et al.*[143] synthesized SERS-encoded aggregates which, after post-differential centrifugations, yielded large ensembles of clusters selectively enriched in monomers, dimers and trimers yielding reproducible enhancements, in order to provide a more statistically significant comparison between the relative SERS performance of each structure.

Lee *et al.*[209] exploited the surface properties of GNRs to exercise great control over the generation of hot spots, promoting the nanoparticle assembly in a well-ordered end-to-end fashion and the specific localization of the Raman reporter at the interparticle junction (Fig. 18a). The dynamic generation of hot-spots during the progressive enlargement of the self-assembled GNR chains (Fig. 18b) was monitored by measuring both the average plasmonic (Fig. 18c) and SERS responses, which were eventually correlated to the average number of GNR units in the chain, X_n. In Fig. 18d, the normalized SERS intensity and the product of the extinction at 785 nm and 821 nm show strong qualitative correlation when plotted as a function of X_n. which was further supported by theoretical calculations. The extinction values at 785 nm, corresponding to the excitation wavelength, and at 821 nm, corresponding to the scattered Raman Stokes frequency of the Raman band at 563 cm^{-1} (spectral marker for the SERS intensity), were selected according to the expression of SERS-EF as reported in eqn (1), as they are expected to be intrinsically related to the enhancement performance of the nanostructure.

Nonetheless, ensembles of aggregated colloidal nanoparticles characterized by inherent geometrical and/or interparticle gap inhomogeneity are still largely used in the scientific community as highly effective SERS enhancing substrates in a large variety of applications. The extended broadening of extinction spectra

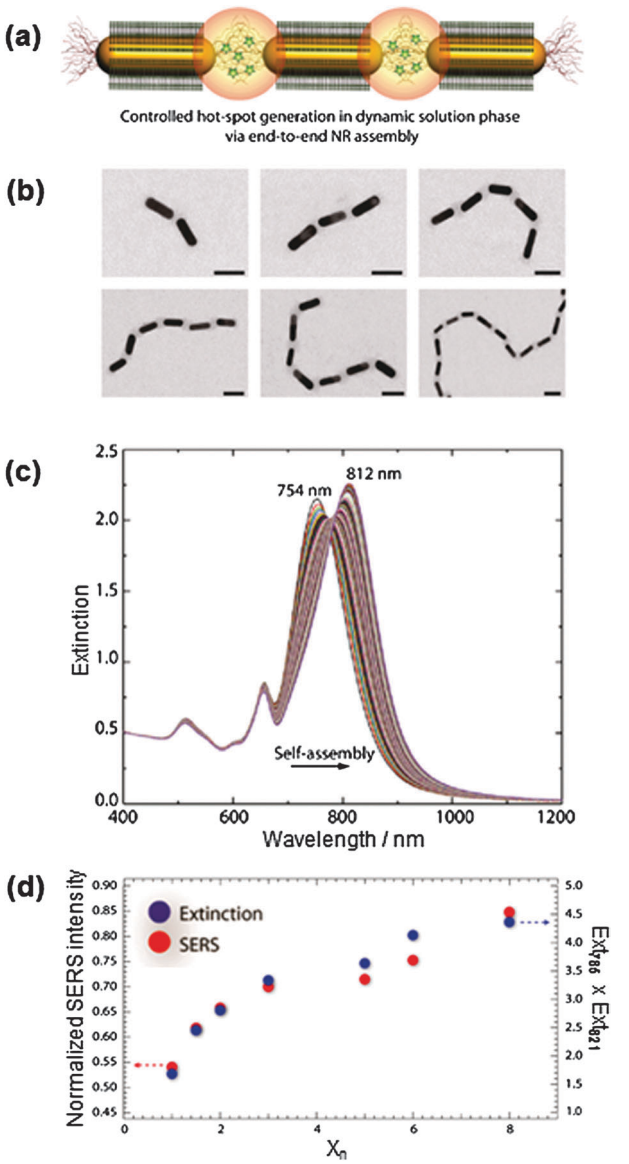

Fig. 18 (a) Schematic of the generation of hot-spots *via* end-to-end self-assembly of gold nanorods (GNRs) in chains with the inclusion of a Raman reporter at the interparticle junctions. (b) Representative STEM images of the self-assembled chains of GNRs (scale bar is 40 nm). (c) Variation in extinction properties of NRs in the course of their self-assembly in chains. (d) Correlation of the normalized SERS intensity and the product of extinctions measured at 785 and 821 nm plotted as a function of the average aggregation number X_n of the GNR chains. Adapted with permission from ref. 209. Copyright 2011, American Chemical Society.

observed when colloidal nanoparticles progressively aggregate into larger structures of different sizes is the result of the superimposition of the individual characteristic plasmon contribution of each individual cluster in suspension. As previously pointed out, dimers are arguably the simplest nanoparticle assembly and can be considered as the 'hot-spot unity' within larger clusters. Theoretical models[51,121,123] indicate that red-shifted resonances arising from plasmonic coupling of interacting nanoparticles in dimers (gap-plasmon resonances) are highly sensitive to the excitation geometry, which results in weaker and broader gap-plasmon contributions as compared to those associated with single nanoparticles. Therefore, in large ensembles of nanoparticle clusters those gap-plasmon resonances that have a major impact on the SERS enhancement appear in the extinction spectrum largely hidden by more intense contributions from monomeric nanoparticles and, to a much smaller extent, by "single particle-like" resonances occurring for a polarization direction of the incident light perpendicular to the interparticle axis (see Fig. 5). Based on this theoretical support, careful subtraction of the LSPR band ascribed to monomeric spherical nanoparticles to broad plasmon bands of large ensembles of clusters was carried out in several nanoparticle assembly studies to make emerge plasmon features specifically ascribed to dimer and larger clusters contributions and investigate the role of the bifunctional linker in the hot spot architecture.[154,155,210]

For instance, Taylor *et al.*[211] monitored the dynamic evolution of plasmon and SERS properties in gold nanoparticle assemblies mediated by the Raman-active bifunctional linker Cucurbit[5]uril (CB5) whose rigid barrel-shaped structure carefully fixes the interparticle separation at 0.9 nm. High linker/nanoparticle molar ratios determine a diffusion-limited colloidal growth (DLCA), which results in the preferred formation of chain-like aggregates, whereas lower ratios promote a reaction-limited kinetic assembly (RLCA), characterized by clusters with a more compact globular-like geometry. Fig. 19 illustrates the

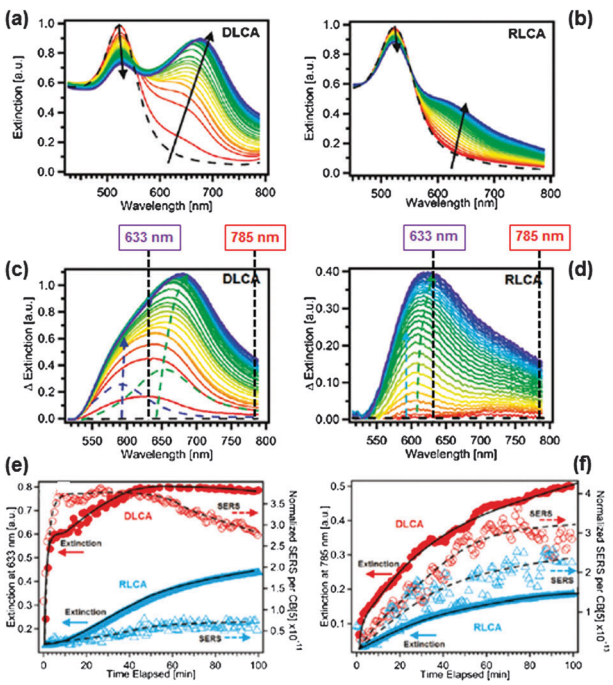

Fig. 19 (a, b) Time-resolved extinction spectra of aggregating AuNP:CB[5] samples for (a) DLCA and (b) RLCA kinetics. Spectra acquired at 1 min intervals for 2 h. (c, d) Difference spectra obtained from (a, b), respectively, by removing the isolated single AuNP contributions. Extinction difference fits best to sum of two Lorentzian modes (dashed) which grow with time. (e, f) Time-resolved normalized SERS intensity of the 826 cm^{-1} CB[5] Raman mode *vs.* time for excitation wavelengths of (e) 633 nm and (f) 785 nm, correlated with aggregate extinction at the excitation wavelength. Adapted with permission from ref. 211. Copyright 2011, American Chemical Society.

time-resolved extinction spectra (a and b) and the corresponding difference spectra (c and d) of gold nanoparticles assembled by CB5 linkers for DLCA and RLCA regimes. Deconvolution of the difference extinction spectra reveals two different contributions, associated to longitudinal plasmon resonance in dimers at ~590 nm and to larger cluster modes that progressively red-shift during the aggregation process. The notable difference that DLCA and RLCA growth kinetics imposed on the time-dependent plasmon properties of the nanoparticle assembly is expected to be reflected also in the SERS response produced by the aggregates. Fig. 19e and f show the time-dependent evolution of the normalized SERS intensity of the CB5 band at 826 cm^{-1} and the extinction value at the excitation wavelengths (633 nm and 785 nm, respectively). The authors explained the correlation between SERS and plasmon properties in terms of resonant matching of maximal plasmonic coupling of the difference extinction spectra with the Raman excitation wavelength.

In our recent work,[212] we suggested a different interpretation of the underlying correlation between averaged plasmonic and surface-enhanced Raman scattering (SERS) properties of large dynamic nanoparticle assembly, discarding "resonant" effects of the excitation laser wavelength and the red-shifted plasmon resonances to achieve maximum SERS efficiency and focusing more on the average cluster size distribution for given interparticle distances. To investigate the relationship between the dynamic structural properties and the time-dependent averaged plasmon and SERS responses of randomly aggregated nanoparticles in suspension, we exploited the DNA-triplex driven assembly of Raman dye-functionalized oligonucleotide-silver nanoparticle conjugates to tune nanoscale junction distances at the nanometer scale, and control the relative aggregation rate during the assembly process. Target dsDNA included an internal sequence with no complementarity to the nanoparticle probes, formed by 0, 5, 10 and 15 base pairs which rigidly tune the interparticle spacing to increasing distances (Fig. 20a).

Additionally, the relative cluster growth rate was intrinsically controlled by the different hybridization rate of the dsDNA sequences (the aggregation rate is higher with decreasing duplex length). Fig. 20b shows the difference extinction spectra for the case of longer dsDNA. Differently to that reported by Taylor *et al.*[211] for gold nanoparticles, the subtraction reveals two well-defined peaks: the stronger and red-shifted contribution (G band) associated with the formation of interparticle gaps in dimer and larger clusters, and an additional weaker feature at *ca.* 380 nm (Q band), which shows to be otherwise scarcely sensitive to the aggregation dynamics. The Q band can be largely assigned to the ensemble of quadrupolar modes of Ag clusters, with the absence in the Au assembly (Fig. 19c and d) ascribed to the much larger intrinsic absorption of gold below 600 nm.[51] The time-dependent evolution of the G band maxima (Fig. 20c) is characterized by the progressive red-shift up to a plateau value whose relative final position shows to be directly dependent on the dsDNA length (*i.e.* gap distance). Despite the heterogeneity of cluster size and shape in the

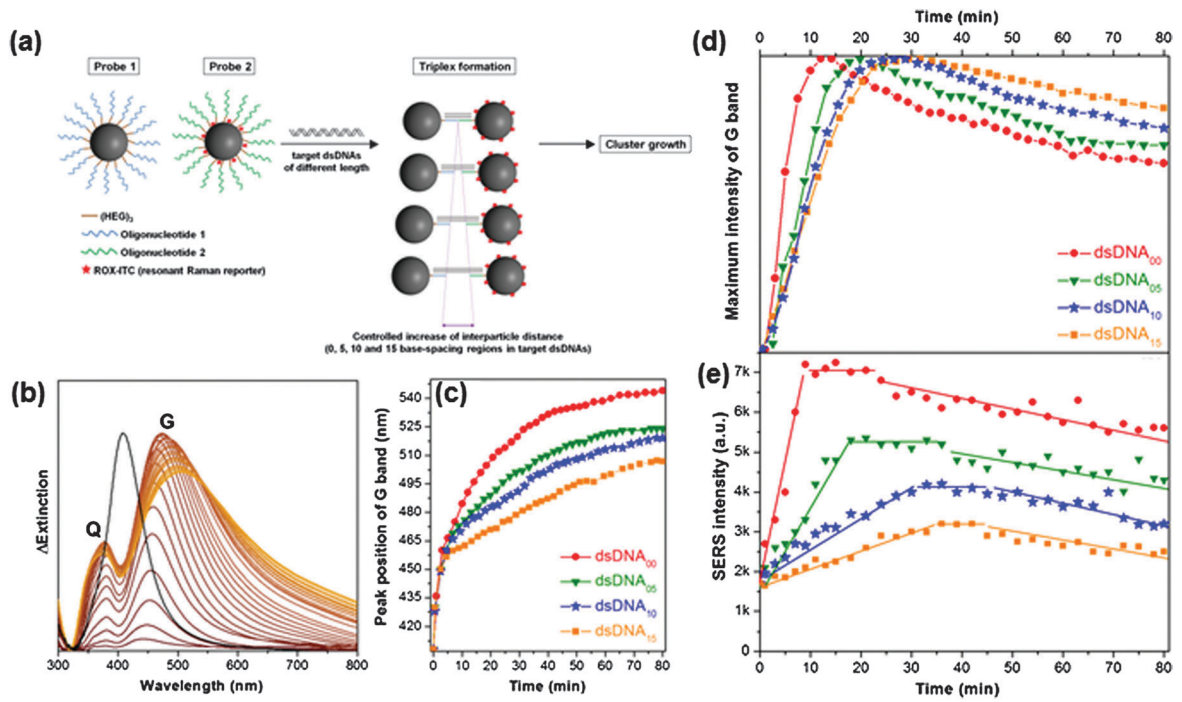

Fig. 20 (a) Outline of the triplex assembly of Raman dye-functionalized oligonucleotide-silver nanoparticles conjugates. (b) Time-dependence evolution of difference extinction spectra obtained by subtracting the extinction spectrum of non-assembled nanoparticle probes from the extinction spectra of the assembled system after the addition of $dsDNA_{15}$. For the sake of comparison, the extinction spectrum at $t = 0$, normalized to the maximum of G band height, is also shown (black line). (c) Peak position of the G band for target dsDNA at different times during the aggregation process. (d) Maximum intensity of the G band (normalized values) and (e) absolute SERS intensity values (peak height of the band at 1646 cm^{-1}) for each dsDNA-driven assembly at different times during the aggregation process. Reproduced from ref. 212 with permission from The Royal Society of Chemistry.

sample and the averaging effect over large ensemble of aggregates, the relative red-shift of the G band is still directly related to the interparticle distance parameter (larger red-shift for shorter interparticle spaces). In addition to this interparticle distance sensitivity, the normalized intensity of the gap-plasmon band shared with the SERS intensity of the dye band at 1646 cm^{-1} (excitation at 532 nm) a similar trend during the aggregation process (Fig. 20d and e). *In situ* kinetic measurements allowed us to evaluate changes in cluster size distribution and relative particle density with statistical reliability, and these were correlated with the bulk plasmonic and SERS responses. These results suggest that at the early stages of the nanoparticle assembly, the G band increases in intensity since dimers/trimers are formed mostly to the detriment of individual nanoparticles (*i.e.* interparticle junctions are generated in the colloidal suspension) until a relevant fraction of these small clusters is itself involved in the aggregation to generate larger structures with broader and weaker plasmonic modes, as revealed by the decrease in the overall plasmon intensity. Similarly, the SERS intensity undergoes an initial steep increase when poorly enhancing monomeric particles are assembled into highly SERS effective dimers/trimers before reaching a plateau and then a slow decrease when small clusters are consumed to form much larger aggregates which, on the one hand, does not improve the SERS performance of the system, as experimentally shown by Wustholz *et al.*[125] and, on the other hand, eventually leads to a decrease of the cluster density in the colloidal volume interrogated by the laser. Importantly, the data reported in Fig. 20e clearly indicate that, even for relatively large interparticle distances as the ones determined by DNA linking, the overall SERS intensity is largely determined by this parameter rather than the cluster size/geometry distribution.

Concluding remarks and outlook

Over the last few years, SERS has experienced a tremendous increase of attention in the scientific community, expanding to a continuously wider range of diverse applications in nanoscience. Previous limitations due to signal irreproducibility and incomplete understanding of the relation between substrate properties and SERS performance have been overcome by significant improvements in nanofabrication techniques, paving the way for the controlled design of reliable and effective SERS nanostructures. Extremely intriguing are the plasmon coupling properties of assembled nanoparticles which concentrate largest electromagnetic enhancements at the interparticle gaps. Recently, great efforts have been devoted to develop new nanoparticle assembly strategies in suspension with improved control over hot-spot architecture and cluster structure, laying the foundation for the full exploitation of their exceptional potential as SERS materials in a wealth of chemical and biological sensing. In this review, we reported an extended description of the advances in plasmonic nanoparticle assembling methods in suspension for a large variety of SERS applications, focusing in particular on those strategies which exploited molecular linkers to engineer interparticle gaps in a controlled manner. An initial general description of the SERS phenomenon together with a theoretical discussion of the plasmon coupling effect for interacting nanoparticles was presented to provide the necessary tools for the critical understanding of the different nanoparticle assembling strategies developed in the literature. The last section was devoted to describe the results of very recent reports focused on unravelling the correlation between average SERS and plasmon responses in large nanoparticle assemblies in suspension, which study is still at its infancy.

As for the most recent nanofabrication advances, there is still much fundamental research to be done in the development of plasmonic nanoparticle assembly methods to design high-quality SERS platforms in a simple and reproducible way, and furthermore to fully exploit their great analytical potential to a well-established practical level. As already mentioned in the manuscript, the specific application for which the SERS substrate is designed *via* assembly strategy in suspension dictates the desired characteristic of the plasmonic support. However, it is possible to individuate some future grand challenges of this relatively new scientific field.

Firstly, extending the control over the fabrication of assemblies with reproducible and known structural properties is of paramount importance to reduce the variability from gap to gap, and cluster to cluster, that limits their applications especially in SERS quantitative analysis. At the same time, efforts should be devoted to simplify these fabrication methods, to facilitate their exploitations beyond those groups with high expertise in the nanofabrication field, which often represents a practical obstacle to their effective use in the myriad of practical potential SERS applications. Secondly, robustness of the assembled system is a key feature to be optimized, in order to prevent alterations of the SERS response due to external *stimuli* non-correlated with the analyte detection. Most of the current strategies impart stability on the nanoparticle clusters by coating with external layers which, however, drastically hamper the accessibility of molecules to the hot spot volume. Thus, more work is required to develop coating strategies, possibly in conjunction with functionalization methods to carefully control the metal surface chemistry, to guarantee cluster stability and selective permeability of the target analyte to the interparticle gap. This would also constitute a great step toward the maximization of the SERS sensitivity preventing large analyte adsorption outside the volume of high enhancements (the hot spot usually represents a very small portion of the total surface area for adsorption). Additionally, the development of methodologies for rapidly characterizing the SERS properties of individual clusters in suspension[153,213–215] is still at its infancy and future intensive research in this area is expected to come.

As a more general consideration, an apparently trivial limitation to the application to real analytical problems of novel SERS platforms, from individual asymmetric nanoparticles to particle assemblies and beyond to structured surfaces, is the lack of a standardized characterization protocol which could effectively provide detailed information about the substrate properties. In the large part of the nanofabrication literature, the SERS performance of newly designed metal structures is probed by assembling monolayers of thiophenol-like molecules or rhodamine-like dyes capable of strongly interacting with the metal surface and generating intense Raman signals.

Although the choice of these reference chemicals is appropriate to test the maximum SERS activity, it provides very limited information to the scientific community of potential SERS users willing to extend the use of the novel substrate to practical applications. We feel that at least the following points should be addressed in a characterization protocol. The affinity of molecules presenting anchoring groups with different affinity to the metal should be investigated to characterize the surface chemistry of the SERS substrate. For instance, a series of substituted benzenes (such as benzoic acid, benzonitrile and aniline, in addition to thiophenol) can be used for this purpose. In addition, concentration studies in the sub-monolayer coverage should be performed to probe the linear response of the metal substrates at different surface concentrations. In fact, if the EM enhancement across the spherical particle is relatively homogenous, asymmetric-shaped nanoparticles or hot-spot containing substrates often show high discrepancy between local enhancements at the surface and, therefore, preferential adsorptions of the analyte under the monolayer coverage may result in non-linear dependence with SERS intensity. In this regard, the analyte accessibility to different areas of the metal substrate should be also tested by progressively increasing the molecule probe size, maintaining the same anchoring group. Finally, different excitation lines should be used, such as 514 nm and 785 nm for silver substrates and 633 nm and 785 nm for gold substrates. This tedious but extended characterization would represent a critical step to rapidly translate the use of novel SERS substrates to real analytical problems, acting also as useful feedback for the development of nanofabrication designs to effectively satisfy the requirements of SERS applications.

Nonetheless, it is undoubtedly a fact that SERS research has finally undertaken the successful path to continue its virtuous progress toward routine application and is set to continue in its growth and adoption for exploitation in a range of meaningful studies and applications and the abovementioned challenges in the nanoparticle assembly strategies for the fabrication of highly effective SERS substrates constitute, on the other hand, a great scientific opportunity awaiting to be explored.

Notes and references

1 V. Giannini, A. I. Fernandez-Dominguez, S. C. Heck and S. A. Maier, *Chem. Rev.*, 2011, **111**, 3888–3912.
2 J. A. Schuller, E. S. Barnard, W. S. Cai, Y. C. Jun, J. S. White and M. L. Brongersma, *Nat. Mater.*, 2010, **9**, 193–204.
3 S. J. Tan, M. J. Campolongo, D. Luo and W. L. Cheng, *Nat. Nanotechnol.*, 2011, **6**, 268–276.
4 S. Lal, N. K. Grady, J. Kundu, C. S. Levin, J. B. Lassiter and N. J. Halas, *Chem. Soc. Rev.*, 2008, **37**, 898–911.
5 J. F. Li, Y. F. Huang, Y. Ding, Z. L. Yang, S. B. Li, X. S. Zhou, F. R. Fan, W. Zhang, Z. Y. Zhou, D. Y. Wu, B. Ren, Z. L. Wang and Z. Q. Tian, *Nature*, 2010, **464**, 392–395.
6 N. P. W. Pieczonka and R. F. Aroca, *Chem. Soc. Rev.*, 2008, **37**, 946–954.
7 I. A. Larmour and D. Graham, *Analyst*, 2011, **136**, 3831–3853.
8 P. P. Pompa, L. Martiradonna, A. Della Torre, F. Della Sala, L. Manna, M. De Vittorio, F. Calabi, R. Cingolani and R. Rinaldi, *Nat. Nanotechnol.*, 2006, **1**, 126–130.
9 J. Zhang, Y. Fu, M. H. Chowdhury and J. R. Lakowicz, *Nano Lett.*, 2007, **7**, 2101–2107.
10 M. Osawa, *Near-Field Optics and Surface Plasmon Polaritons*, 2001, **81**, 163–187.
11 P. Christopher, H. L. Xin and S. Linic, *Nat. Chem.*, 2011, **3**, 467–472.
12 E. M. Larsson, C. Langhammer, I. Zoric and B. Kasemo, *Science*, 2009, **326**, 1091–1094.
13 S. D. Standridge, G. C. Schatz and J. T. Hupp, *J. Am. Chem. Soc.*, 2009, **131**, 8407–8408.
14 L. A. Austin, B. Kang, C. W. Yen and M. A. El-Sayed, *J. Am. Chem. Soc.*, 2011, **133**, 17594–17597.
15 E. C. Dreaden, M. A. Mackey, X. H. Huang, B. Kang and M. A. El-Sayed, *Chem. Soc. Rev.*, 2011, **40**, 3391–3404.
16 K. Wilson, K. Homan and S. Emelianov, *Nat. Commun.*, 2012, **3**.
17 V. Giannini, A. I. Fernandez-Dominguez, Y. Sonnefraud, T. Roschuk, R. Fernandez-Garcia and S. A. Maier, *Small*, 2010, **6**, 2498–2507.
18 N. J. Halas, S. Lal, W. S. Chang, S. Link and P. Nordlander, *Chem. Rev.*, 2011, **111**, 3913–3961.
19 E. C. Le Ru, P. G. Etchegoin and M. Meyer, *J. Chem. Phys.*, 2006, **125**, 204701–204713.
20 K. Kneipp, Y. Wang, H. Kneipp, L. T. Perelman, I. Itzkan, R. Dasari and M. S. Feld, *Phys. Rev. Lett.*, 1997, **78**, 1667–1670.
21 S. Nie and S. R. Emery, *Science*, 1997, **275**, 1102–1106.
22 E. J. Blackie, E. C. Le Ru and P. G. Etchegoin, *J. Am. Chem. Soc.*, 2009, **131**, 14466–14472.
23 E. Blackie, E. C. Le Ru, M. Meyer, M. Timmer, B. Burkett, P. Northcote and P. G. Etchegoin, *Phys. Chem. Chem. Phys.*, 2008, **10**, 4147–4153.
24 D. L. Jeanmaire and R. P. Van Duyne, *J. Electroanal. Chem.*, 1977, **84**, 1–20.
25 M. G. Albrecht and J. A. Creighton, *J. Am. Chem. Soc.*, 1977, **99**, 5215–5217.
26 Z. Q. Tian, *J. Raman Spectrosc.*, 2005, **36**, 466–470.
27 J. A. Dieringer, A. D. McFarland, N. C. Shah, D. A. Stuart, A. V. Whitney, C. R. Yonzon, M. A. Young, X. Y. Zhang and R. P. Van Duyne, *Faraday Discuss.*, 2006, **132**, 9–26.
28 S. E. J. Bell and N. M. S. Sirimuthu, *Chem. Soc. Rev.*, 2008, **37**, 1012–1024.
29 R. J. C. Brown and M. J. T. Milton, *J. Raman Spectrosc.*, 2008, **39**, 1313–1326.
30 H. Ko, S. Singamaneni and V. V. Tsukruk, *Small*, 2008, **4**, 1576–1599.
31 R. A. Tripp, R. A. Dluhy and Y. P. Zhao, *Nano Today*, 2008, **3**, 31–37.
32 W. E. Smith, *Chem. Soc. Rev.*, 2008, **37**, 955–964.
33 M. D. Porter, R. J. Lipert, L. M. Siperko, G. Wang and R. Narayanana, *Chem. Soc. Rev.*, 2008, **37**, 1001–1011.
34 E. Bailo and V. Deckert, *Chem. Soc. Rev.*, 2008, **37**, 921–930.
35 S. Abalde-Cela, P. Aldeanueva-Potel, C. Mateo-Mateo, L. Rodriguez-Lorenzo, R. A. Alvarez-Puebla and L. M. Liz-Marzan, *J. R. Soc., Interface*, 2010, **7**, S435–S450.
36 R. A. Alvarez-Puebla and L. M. Liz-Marzan, *Energy Environ. Sci.*, 2010, **3**, 1011–1017.
37 J. A. Dougan and K. Faulds, *Analyst*, 2012, **137**, 545–554.
38 R. A. Alvarez-Puebla and L. M. Liz-Marzan, *Chem. Soc. Rev.*, 2012, **41**, 43–51.
39 I. A. Larmour, K. Faulds and D. Graham, *Chem. Sci.*, 2010, **1**, 151–160.
40 A. Gopinath, S. V. Boriskina, W. R. Premasiri, L. Ziegler, B. M. Reinhard and L. Dal Negro, *Nano Lett.*, 2009, **9**, 3922–3929.
41 A. Sanchez-Iglesias, P. Aldeanueva-Potel, W. H. Ni, J. Perez-Juste, I. Pastoriza-Santos, R. A. Alvarez-Puebla, B. N. Mbenkum and L. M. Liz-Marzan, *Nano Today*, 2010, **5**, 21–27.
42 C. L. Haynes and R. P. Van Duyne, *J. Phys. Chem. B*, 2001, **105**, 5599–5611.
43 R. J. Stokes, J. A. Dougan and D. Graham, *Chem. Commun.*, 2008, 5734–5736.
44 Y. Lu, G. L. Liu and L. P. Lee, *Nano Lett.*, 2005, **5**, 5–9.
45 H. Wang, C. S. Levin and N. J. Halas, *J. Am. Chem. Soc.*, 2005, **127**, 14992–14993.
46 A. Q. Chen, A. E. DePrince, A. Demortiere, A. Joshi-Imre, E. V. Shevchenko, S. K. Gray, U. Welp and V. K. Vlasko-Vlasov, *Small*, 2011, **7**, 2365–2371.
47 Z. N. Zhu, H. F. Meng, W. J. Liu, X. F. Liu, J. X. Gong, X. H. Qiu, L. Jiang, D. Wang and Z. Y. Tang, *Angew. Chem., Int. Ed.*, 2011, **50**, 1593–1596.

48 N. Pazos-Perez, W. H. Ni, A. Schweikart, R. A. Alvarez-Puebla, A. Fery and L. M. Liz-Marzan, *Chem. Sci.*, 2010, **1**, 174–178.
49 J. M. Romo-Herrera, R. A. Alvarez-Puebla and L. M. Liz-Marzan, *Nanoscale*, 2011, **3**, 1304–1315.
50 D. A. Long, *Raman Spectroscopy*, Maidenhead, Gt. Britain, 1977.
51 E. C. Le Ru and P. G. Etchegoin, *Principles of Surface-Enhanced Raman Spectroscopy*, Elsevier, Amsterdam, 2009.
52 S. P. Mulvaney and C. D. Keating, *Anal. Chem.*, 2000, **72**, 145R–157R.
53 K. Kneipp, H. Kneipp, I. Itzkan, R. R. Dasari and M. S. Feld, *Chem. Rev.*, 1999, **99**, 2957–2975.
54 W. Kiefer, *J. Raman Spectrosc.*, 2007, **38**, 1538–1553.
55 M. Fleischmann, P. J. Hendra and A. J. McQuillan, *Chem. Phys. Lett.*, 1974, **26**, 163–166.
56 R. Aroca, *Surface-enhanced Vibrational Spectroscopy*, John Wiley & Sons, Chichester, 2006.
57 Y. Zhang, H. Hong, D. V. Myklejord and W. B. Cai, *Small*, 2011, **7**, 3261–3269.
58 R. S. Golightly, W. E. Doering and M. J. Natan, *ACS Nano*, 2009, **3**, 2859–2869.
59 K. L. Wustholz, C. L. Brosseau, F. Casadio and R. P. Van Duyne, *Phys. Chem. Chem. Phys.*, 2009, **11**, 7350–7359.
60 Z. Q. Tian, B. Ren, J. F. Li and Z. L. Yang, *Chem. Commun.*, 2007, 3514–3534.
61 D. Graham and K. Faulds, *Chem. Soc. Rev.*, 2008, **37**, 1042–1051.
62 X. M. Qian and S. M. Nie, *Chem. Soc. Rev.*, 2008, **37**, 912–920.
63 S. Schlucker, *ChemPhysChem*, 2009, **10**, 1344–1354.
64 H. Kim, K. M. Kosuda, R. P. Van Duyne and P. C. Stair, *Chem. Soc. Rev.*, 2010, **39**, 4820–4844.
65 L. M. Tong, T. Zhu and Z. F. Liu, *Chem. Soc. Rev.*, 2011, **40**, 1296–1304.
66 E. C. Le Ru, E. Blackie, M. Meyer and P. G. Etchegoin, *J. Phys. Chem. C*, 2007, **111**, 13794–13803.
67 M. Moskovits, *Rev. Mod. Phys.*, 1985, **57**, 783–826.
68 E. C. Le Ru and P. G. Etchegoin, *Chem. Phys. Lett.*, 2006, **423**, 63–66.
69 X. P. Gao, J. P. Davies and M. J. Weaver, *J. Phys. Chem.*, 1990, **94**, 6858–6864.
70 M. Moskovits, *J. Chem. Phys.*, 1982, **77**, 4408–4416.
71 E. C. Le Ru and P. G. Etchegoin, *Annu. Rev. Phys. Chem.*, 2012, **63**, 65–87.
72 D. K. Lim, K. S. Jeon, H. M. Kim, J. M. Nam and Y. D. Suh, *Nat. Mater.*, 2010, **9**, 60–67.
73 T. Dadosh, J. Sperling, G. W. Bryant, R. Breslow, T. Shegai, M. Dyshel, G. Haran and I. Bar-Joseph, *ACS Nano*, 2009, **3**, 1988–1994.
74 C. J. Murphy, A. M. Gole, J. W. Stone, P. N. Sisco, A. M. Alkilany, E. C. Goldsmith and S. C. Baxter, *Acc. Chem. Res.*, 2008, **41**, 1721–1730.
75 J. P. Camden, J. A. Dieringer, J. Zhao and R. P. Van Duyne, *Acc. Chem. Res.*, 2008, **41**, 1653–1661.
76 R. A. Alvarez-Puebla and L. M. Liz-Marzan, *Small*, 2010, **6**, 604–610.
77 D. Graham, K. Faulds, D. Thompson, F. McKenzie, R. Stokes, C. Dalton, R. Stevenson, J. Alexander, P. Garside and E. McFarlane, *Biochem. Soc. Trans.*, 2009, **37**, 697–701.
78 T. R. Jensen, M. D. Malinsky, C. L. Haynes and R. P. Van Duyne, *J. Phys. Chem. B*, 2000, **104**, 10549–10556.
79 P. Tessier, O. D. Velev, A. T. Kalambur, A. M. Lenhoff, J. F. Rabolt and E. W. Kaler, *Adv. Mater.*, 2001, **13**, 396–400.
80 M. J. Banholzer, J. E. Millstone, L. D. Qin and C. A. Mirkin, *Chem. Soc. Rev.*, 2008, **37**, 885–897.
81 L. Guerrini, J. V. Garcia-Ramos, C. Domingo and S. Sanchez-Cortes, *Anal. Chem.*, 2009, **81**, 953–960.
82 L. Guerrini, J. V. Garcia-Ramos, C. Domingo and S. Sanchez-Cortes, *Langmuir*, 2006, **22**, 10924–10926.
83 Y. F. Xie, X. Wang, X. X. Han, X. X. Xue, W. Ji, Z. H. Qi, J. Q. Liu, B. Zhao and Y. Ozaki, *Analyst*, 2010, **135**, 1389–1394.
84 C. A. Tao, Q. An, W. Zhu, H. W. Yang, W. N. Li, C. X. Lin, D. Xu and G. T. Li, *Chem. Commun.*, 2011, **47**, 9867–9869.
85 S. J. Lee and M. Moskovits, *Nano Lett.*, 2011, **11**, 145–150.
86 D. Grasseschi, V. M. Zamarion, K. Araki and H. E. Toma, *Anal. Chem.*, 2010, **82**, 9146–9149.
87 D. Tsoutsi, J. M. Montenegro, F. Dommershausen, U. Koert, L. M. Liz-Marzan, W. J. Perak and R. A. Alvarez-Puebla, *ACS Nano*, 2011, **5**, 7539–7546.
88 S. W. Bishnoi, C. J. Rozell, C. S. Levin, M. K. Gheith, B. R. Johnson, D. H. Johnson and N. J. Halas, *Nano Lett.*, 2006, **6**, 1687–1692.
89 A. Pallaoro, G. B. Braun, N. O. Reich and M. Moskovits, *Small*, 2009, **6**, 618–622.
90 Z. Krpetic, L. Guerrini, I. A. Larmour, R. Reglinski, K. Faulds and D. Graham, *Small*, 2012, **8**, 707–714.
91 P. C. Lee and D. Meisel, *J. Phys. Chem.*, 1982, **86**, 3391–3395.
92 X. M. Lu, M. Rycenga, S. E. Skrabalak, B. Wiley and Y. N. Xia, *Annu. Rev. Phys. Chem.*, 2009, **60**, 167–192.
93 C. Fernandez-Lopez, C. Mateo-Mateo, R. A. Alvarez-Puebla, J. Perez-Juste, I. Pastoriza-Santos and L. M. Liz-Marzan, *Langmuir*, 2009, **25**, 13894–13899.
94 H. Y. Guo, F. X. Ruan, L. H. Lu, J. W. Hu, J. A. Pan, Z. L. Yang and B. Ren, *J. Phys. Chem. C*, 2009, **113**, 10459–10464.
95 R. A. Alvarez-Puebla, A. Agarwal, P. Manna, B. P. Khanal, P. Aldeanueva-Potel, E. Carbo-Argibay, N. Pazos-Perez, L. Vigderman, E. R. Zubarev, N. A. Kotov and L. M. Liz-Marzan, *Proc. Natl. Acad. Sci. U. S. A.*, 2011, **108**, 8157–8161.
96 G. von Maltzahn, A. Centrone, J. H. Park, R. Ramanathan, M. J. Sailor, T. A. Hatton and S. N. Bhatia, *Adv. Mater.*, 2009, **21**, 3175–3180.
97 X. H. Huang, S. Neretina and M. A. El-Sayed, *Adv. Mater.*, 2009, **21**, 4880–4910.
98 J. M. McLellan, Z. Y. Li, A. R. Siekkinen and Y. N. Xia, *Nano Lett.*, 2007, **7**, 1013–1017.
99 M. Rycenga, X. H. Xia, C. H. Moran, F. Zhou, D. Qin, Z. Y. Li and Y. A. Xia, *Angew. Chem., Int. Ed.*, 2011, **50**, 5473–5477.
100 I. Pastoriza-Santos and L. M. Liz-Marzan, *J. Mater. Chem.*, 2008, **18**, 1724–1737.
101 F. Hao, Y. Sonnefraud, P. Van Dorpe, S. A. Maier, N. J. Halas and P. Nordlander, *Nano Lett.*, 2008, **8**, 3983–3988.
102 L. Rodriguez-Lorenzo, R. A. Alvarez-Puebla, F. J. G. de Abajo and L. M. Liz-Marzan, *J. Phys. Chem. C*, 2010, **114**, 7336–7340.
103 L. Rodriguez-Lorenzo, Z. Krpetic, S. Barbosa, R. A. Alvarez-Puebla, L. M. Liz-Marzan, I. A. Prior and M. Brust, *Integr. Biol.*, 2011, **3**, 922–926.
104 D. S. dos Santos, R. A. Alvarez-Puebla, O. N. Oliveira and R. F. Aroca, *J. Mater. Chem.*, 2005, **15**, 3045–3049.
105 L. R. Hirsch, A. M. Gobin, A. R. Lowery, F. Tam, R. A. Drezek, N. J. Halas and J. L. West, *Ann. Biomed. Eng.*, 2006, **34**, 15–22.
106 W. B. Li, X. Y. Miao, T. S. Luk and P. Zhang, *J. Phys. Chem. C*, 2011, **115**, 3318–3326.
107 P. Zhang and Y. Y. Guo, *J. Am. Chem. Soc.*, 2009, **131**, 3808–3809.
108 B. Kustner, M. Gellner, M. Schutz, F. Schoppler, A. Marx, P. Strobel, P. Adam, C. Schmuck and S. Schlucker, *Angew. Chem., Int. Ed.*, 2009, **48**, 1950–1953.
109 E. C. Le Ru, J. Grand, I. Sow, W. R. C. Somerville, P. G. Etchegoin, M. Treguer-Delapierre, G. Charron, N. Felidj, G. Levi and J. Aubard, *Nano Lett.*, 2011, **11**, 5013–5019.
110 V. Giannini, R. Rodriguez-Oliveros and J. A. Sanchez-Gil, *Plasmonics*, 2010, **5**, 99–104.
111 H. N. Xie, I. A. Larmour, V. Tileli, A. L. Koh, D. W. McComb, K. Faulds and D. Graham, *J. Phys. Chem. C*, 2011, **115**, 20515–20522.
112 R. Alvarez-Puebla, L. M. Liz-Marzan and F. J. G. de Abajo, *J. Phys. Chem. Lett.*, 2010, **1**, 2428–2434.
113 L. Rodriguez-Lorenzo, R. A. Alvarez-Puebla, I. Pastoriza-Santos, S. Mazzucco, O. Stephan, M. Kociak, L. M. Liz-Marzan and F. J. G. de Abajo, *J. Am. Chem. Soc.*, 2009, **131**, 4616–4618.
114 F. Hao, C. L. Nehl, J. H. Hafner and P. Nordlander, *Nano Lett.*, 2007, **7**, 729–732.
115 M. J. Mulvihill, X. Y. Ling, J. Henzie and P. D. Yang, *J. Am. Chem. Soc.*, 2010, **132**, 268–274.
116 M. Yang, R. Alvarez-Puebla, H. S. Kim, P. Aldeanueva-Potel, L. M. Liz-Marzan and N. A. Kotov, *Nano Lett.*, 2010, **10**, 4013–4019.
117 D. K. Lim, K. S. Jeon, J. H. Hwang, H. Kim, S. Kwon, Y. D. Suh and J. M. Nam, *Nat. Nanotechnol.*, 2011, **6**, 452–460.
118 A. Biswas, T. Wang and A. S. Biris, *Nanoscale*, 2010, **2**, 1560–1572.
119 M. Grzelczak, J. Perez-Juste, P. Mulvaney and L. M. Liz-Marzan, *Chem. Soc. Rev.*, 2008, **37**, 1783–1791.
120 L. Guerrini, Z. Jurasekova, C. Domingo, M. Perez-Mendez, P. Leyton, M. Campos-Vallette, J. V. Garcia-Ramos and S. Sanchez-Cortes, *Plasmonics*, 2007, **2**, 147–156.

121 E. Hao and G. C. Schatz, *J. Chem. Phys.*, 2004, **120**, 357–366.
122 E. R. Encina and E. A. Coronado, *J. Phys. Chem. C*, 2010, **114**, 3918–3923.
123 E. C. Le Ru, C. Galloway and P. G. Etchegoin, *Phys. Chem. Chem. Phys.*, 2006, **8**, 3083–3087.
124 C. E. Talley, J. B. Jackson, C. Oubre, N. K. Grady, C. W. Hollars, S. M. Lane, T. R. Huser, P. Nordlander and N. J. Halas, *Nano Lett.*, 2005, **5**, 1569–1574.
125 K. L. Wustholz, A. I. Henry, J. M. McMahon, R. G. Freeman, N. Valley, M. E. Piotti, M. J. Natan, G. C. Schatz and R. P. Van Duyne, *J. Am. Chem. Soc.*, 2010, **132**, 10903–10910.
126 D. F. Evans and H. Wennerström, *The colloidal domains: where physics, chemistry, biology and technology meet.*, Wiley-VHC, New York, 1999.
127 S. E. J. Bell and N. M. S. Sirimuthu, *J. Am. Chem. Soc.*, 2006, **128**, 15580–15581.
128 A. Otto, A. Bruckbauer and Y. X. Chen, *J. Mol. Struct.*, 2003, **661**, 501–514.
129 R. L. Garrell, K. D. Shaw and S. Krimm, *Surf. Sci.*, 1983, **124**, 613–624.
130 J. Turkevich, P. C. Stevenson and J. Hillier, *Discuss. Faraday Soc.*, 1951, 55–75.
131 N. Leopold and B. Lendl, *J. Phys. Chem. B*, 2003, **107**, 5723–5727.
132 S. M. Heard, F. Grieser, C. G. Barraclough and J. V. Sanders, *J. Colloid Interface Sci.*, 1983, **93**, 545–555.
133 D. Graham, W. E. Smith, A. M. T. Linacre, C. H. Munro, N. D. Watson and P. C. White, *Anal. Chem.*, 1997, **69**, 4703–4707.
134 C. H. Munro, W. E. Smith, M. Garner, J. Clarkson and P. C. White, *Langmuir*, 1995, **11**, 3712–3720.
135 S. E. J. Bell and M. R. McCourt, *Phys. Chem. Chem. Phys.*, 2009, **11**, 7455–7462.
136 M. Meyer, E. C. Le Ru and P. G. Etchegoin, *J. Phys. Chem. B*, 2006, **110**, 6040–6047.
137 P. G. Etchegoin, M. Meyer, E. Blackie and E. C. Le Ru, *Anal. Chem.*, 2007, **79**, 8411–8415.
138 E. C. Le Ru, M. Meyer and P. G. Etchegoin, *J. Phys. Chem. B*, 2006, **110**, 1944–1948.
139 W. Y. Li, P. H. C. Camargo, X. M. Lu and Y. N. Xia, *Nano Lett.*, 2009, **9**, 485–490.
140 W. Y. Li, P. H. C. Camargo, L. Au, Q. Zhang, M. Rycenga and Y. N. Xia, *Angew. Chem., Int. Ed.*, 2010, **49**, 164–168.
141 I. A. Larmour, K. Faulds and D. Graham, *J. Phys. Chem. C*, 2010, **114**, 13249–13254.
142 X. J. Wang, G. P. Li, T. Chen, M. X. Yang, Z. Zhang, T. Wu and H. Y. Chen, *Nano Lett.*, 2008, **8**, 2643–2647.
143 G. Chen, Y. Wang, M. X. Yang, J. Xu, S. J. Goh, M. Pan and H. Y. Chen, *J. Am. Chem. Soc.*, 2010, **132**, 3644–3645.
144 D. Steinigeweg, M. Schutz, M. Salehi and S. Schlucker, *Small*, 2011, **7**, 2443–2448.
145 L. Rocks, K. Faulds and D. Graham, *Chem. Commun.*, 2011, **47**, 4415–4417.
146 D. J. Anderson and M. Moskovits, *J. Phys. Chem. B*, 2006, **110**, 13722–13727.
147 S. J. Lee, A. R. Morrill and M. Moskovits, *J. Am. Chem. Soc.*, 2006, **128**, 2200–2201.
148 G. Braun, I. Pavel, A. R. Morrill, D. S. Seferos, G. C. Bazan, N. O. Reich and M. Moskovits, *J. Am. Chem. Soc.*, 2007, **129**, 7760.
149 B. Vlckova, M. Moskovits, I. Pavel, K. Siskova, M. Sladkova and M. Slouf, *Chem. Phys. Lett.*, 2008, **455**, 131–134.
150 D. D. Whitmore, P. Z. El-Khoury, L. Fabris, P. Chu, G. C. Bazan, E. O. Potma and V. A. Apkarian, *J. Phys. Chem. C*, 2011, **115**, 15900–15907.
151 L. Fabris, M. Dante, T. Q. Nguyen, J. B. H. Tok and G. C. Bazan, *Adv. Funct. Mater.*, 2008, **18**, 2518–2525.
152 G. B. Braun, S. J. Lee, T. Laurence, N. Fera, L. Fabris, G. C. Bazan, M. Moskovits and N. O. Reich, *J. Phys. Chem. C*, 2009, **113**, 13622–13629.
153 T. A. Laurence, G. Braun, C. Talley, A. Schwartzberg, M. Moskovits, N. Reich and T. Huser, *J. Am. Chem. Soc.*, 2009, **131**, 162–169.
154 L. Guerrini, I. Izquierdo-Lorenzo, R. Rodriguez-Oliveros, J. A. Sanchez-Gil, S. Sanchez-Cortes, J. V. Garcia-Ramos and C. Domingo, *Plasmonics*, 2010, **5**, 273–286.
155 L. Guerrini, J. V. Garcia-Ramos, C. Domingo and S. Sanchez-Cortes, *J. Phys. Chem. C*, 2008, **112**, 7527–7530.
156 L. Guerrini, J. V. Garcia-Ramos, C. Domingo and S. Sanchez-Cortes, *Anal. Chem.*, 2009, **81**, 1418–1425.
157 L. Guerrini, J. V. Garcia-Ramos, C. Domingo and S. Sanchez-Cortes, *Phys. Chem. Chem. Phys.*, 2009, **11**, 1787–1793.
158 P. Leyton, S. Sanchez-Cortes, J. V. Garcia-Ramos, C. Domingo, M. Campos-Vallette, C. Saitz and R. E. Clavijo, *J. Phys. Chem. B*, 2004, **108**, 17484–17490.
159 H. Yan, S. I. Lim, L. C. Zhang, S. C. Gao, D. Mott, Y. A. Le, R. Loukrakpam, D. L. An and C. J. Zhong, *J. Mater. Chem.*, 2011, **21**, 1890–1901.
160 S. S. R. Dasary, A. K. Singh, D. Senapati, H. T. Yu and P. C. Ray, *J. Am. Chem. Soc.*, 2009, **131**, 13806–13812.
161 X. M. Qian, J. Li and S. M. Nie, *J. Am. Chem. Soc.*, 2009, **131**, 7540–7541.
162 P. Taladriz-Blanco, N. J. Buurma, L. Rodriguez-Lorenzo, J. Perez-Juste, L. M. Liz-Marzan and P. Herves, *J. Mater. Chem.*, 2011, **21**, 16880–16887.
163 S. C. Glotzer and M. J. Solomon, *Nat. Mater.*, 2007, **6**, 557–562.
164 M. R. Jones, R. J. Macfarlane, B. Lee, J. A. Zhang, K. L. Young, A. J. Senesi and C. A. Mirkin, *Nat. Mater.*, 2010, **9**, 913–917.
165 W. S. Kuo, C. N. Chang, Y. T. Chang, M. H. Yang, Y. H. Chien, S. J. Chen and C. S. Yeh, *Angew. Chem., Int. Ed.*, 2010, **49**, 2711–2715.
166 L. B. Zhong, X. Zhou, S. X. Bao, Y. F. Shi, Y. Wang, S. M. Hong, Y. C. Huang, X. Wang, Z. X. Xie and Q. Q. Zhang, *J. Mater. Chem.*, 2011, **21**, 14448–14455.
167 T. S. Sreeprasad and T. Pradeep, *Langmuir*, 2011, **27**, 3381–3390.
168 A. McLintock, N. Hunt and A. W. Wark, *Chem. Commun.*, 2011, **47**, 3757–3759.
169 T. Chen, H. Wang, G. Chen, Y. Wang, Y. H. Feng, W. S. Teo, T. Wu and H. Y. Chen, *ACS Nano*, 2010, **4**, 3087–3094.
170 M. M. Maye, D. Nykypanchuk, M. Cuisinier, D. van der Lelie and O. Gang, *Nat. Mater.*, 2009, **8**, 388–391.
171 S. Bidault, F. J. G. de Abajo and A. Polman, *J. Am. Chem. Soc.*, 2008, **130**, 2750–2751.
172 C. J. Loweth, W. B. Caldwell, X. G. Peng, A. P. Alivisatos and P. G. Schultz, *Angew. Chem., Int. Ed.*, 1999, **38**, 1808–1812.
173 A. P. Alivisatos, K. P. Johnsson, X. G. Peng, T. E. Wilson, C. J. Loweth, M. P. Bruchez and P. G. Schultz, *Nature*, 1996, **382**, 609–611.
174 F. A. Aldaye and H. F. Sleiman, *J. Am. Chem. Soc.*, 2007, **129**, 4130–4131.
175 S. Y. Park, A. K. R. Lytton-Jean, B. Lee, S. Weigand, G. C. Schatz and C. A. Mirkin, *Nature*, 2008, **451**, 553–556.
176 C. A. Mirkin, R. L. Letsinger, R. C. Mucic and J. J. Storhoff, *Nature*, 1996, **382**, 607–609.
177 D. Graham, D. G. Thompson, W. E. Smith and K. Faulds, *Nat. Nanotechnol.*, 2008, **3**, 548–551.
178 J. P. Zhang, Y. Liu, Y. G. Ke and H. Yan, *Nano Lett.*, 2006, **6**, 248–251.
179 Z. X. Deng, Y. Tian, S. H. Lee, A. E. Ribbe and C. D. Mao, *Angew. Chem., Int. Ed.*, 2005, **44**, 3582–3585.
180 D. Nykypanchuk, M. M. Maye, D. van der Lelie and O. Gang, *Nature*, 2008, **451**, 549–552.
181 M. M. Maye, M. T. Kumara, D. Nykypanchuk, W. B. Sherman and O. Gang, *Nat. Nanotechnol.*, 2010, **5**, 116–120.
182 X. M. Qian, X. Zhou and S. M. Nie, *J. Am. Chem. Soc.*, 2008, **130**, 14934–14935.
183 D. G. Thompson, K. Faulds, W. E. Smith and D. Graham, *J. Phys. Chem. C*, 2010, **114**, 7384–7389.
184 S. Mahajan, J. Richardson, T. Brown and P. N. Bartlett, *J. Am. Chem. Soc.*, 2008, **130**, 15589–15601.
185 J. Hu, P. C. Zheng, J. H. Jiang, G. L. Shen, R. Q. Yu and G. K. Liu, *Analyst*, 2010, **135**, 1084–1089.
186 G. Braun, S. J. Lee, M. Dante, T. Q. Nguyen, M. Moskovits and N. Reich, *J. Am. Chem. Soc.*, 2007, **129**, 6378–6379.
187 T. Kang, S. M. Yoo, I. Yoon, S. Y. Lee and B. Kim, *Nano Lett.*, 2010, **10**, 1189–1193.
188 S. Q. Sun, D. Thompson, U. Schmidt, D. Graham and G. J. Leggett, *Chem. Commun.*, 2010, **46**, 5292–5294.
189 H. Zhang, M. H. Harpster, H. J. Park and P. A. Johnson, *Anal. Chem.*, 2011, **83**, 254–260.
190 Z. L. Zhang, Y. Q. Wen, Y. Ma, J. Luo, L. Jiang and Y. L. Song, *Chem. Commun.*, 2011, **47**, 7407–7409.

191 N. T. B. Thuy, R. Yokogawa, Y. Yoshimura, K. Fujimoto, M. Koyano and S. Maenosono, *Analyst*, 2010, **135**, 595–602.
192 H. N. Wang and T. Vo-Dinh, *Small*, 2011, **7**, 3067–3074.
193 D. Graham, R. Stevenson, D. G. Thompson, L. Barrett, C. Dalton and K. Faulds, *Faraday Discuss.*, 2011, **149**, 291–299.
194 L. Barrett, J. A. Dougan, K. Faulds and D. Graham, *Nanoscale*, 2011, **3**, 3221–3227.
195 F. McKenzie and D. Graham, *Chem. Commun.*, 2009, 5757–5759.
196 Z. Krpetic, I. Singh, W. Su, L. Guerrini, K. Faulds, G. A. Burley and D. Graham, *J. Am. Chem. Soc.*, 2012, **134**, 8356–8359.
197 Y. L. Wang, K. Lee and J. Irudayaraj, *Chem. Commun.*, 2010, **46**, 613–615.
198 A. J. Bonham, G. Braun, I. Pavel, M. Moskovits and N. O. Reich, *J. Am. Chem. Soc.*, 2007, **129**, 14572–14573.
199 F. McKenzie, K. Faulds and D. Graham, *Chem. Commun.*, 2008, 2367–2369.
200 M. S. Han, A. K. R. Lytton-Jean and C. A. Mirkin, *J. Am. Chem. Soc.*, 2006, **128**, 4954–4955.
201 Y. Chen and C. D. Mao, *Small*, 2008, **4**, 2191–2194.
202 S. Y. Chen and A. A. Lazarides, *J. Phys. Chem. C*, 2009, **113**, 12167–12175.
203 F. McKenzie, K. Faulds and D. Graham, *Small*, 2007, **3**, 1866–1868.
204 J. Wengel, *Acc. Chem. Res.*, 1999, **32**, 301–310.
205 Z. L. Zhang, Y. Q. Wen, Y. Ma, J. Luo, X. Y. Zhang, L. Jiang and Y. L. Song, *Appl. Phys. Lett.*, 2011, **98**, 133704.
206 I. Pavel, E. McCarney, A. Elkhaled, A. Morrill, K. Plaxco and M. Moskovits, *J. Phys. Chem. C*, 2008, **112**, 4880–4883.
207 J. P. Camden, J. A. Dieringer, Y. M. Wang, D. J. Masiello, L. D. Marks, G. C. Schatz and R. P. Van Duyne, *J. Am. Chem. Soc.*, 2008, **130**, 12616–12617.
208 K. A. Stoerzinger, J. Y. Lin and T. W. Odom, *Chem. Sci.*, 2011, **2**, 1435–1439.
209 A. Lee, G. F. S. Andrade, A. Ahmed, M. L. Souza, N. Coombs, E. Tumarkin, K. Liu, R. Gordon, A. G. Brolo and E. Kurnacheva, *J. Am. Chem. Soc.*, 2011, **133**, 7563–7570.
210 L. Guerrini, I. Izquierdo-Lorenzo, J. V. Garcia-Ramos, C. Domingo and S. Sanchez-Cortes, *Phys. Chem. Chem. Phys.*, 2009, **11**, 7363–7371.
211 R. W. Taylor, T. C. Lee, O. A. Scherman, R. Esteban, J. Aizpurua, F. M. Huang, J. J. Baumberg and S. Mahajan, *ACS Nano*, 2011, **5**, 3878–3887.
212 L. Guerrini, F. McKenzie, A. W. Wark, K. Faulds and D. Graham, *Chem. Sci.*, 2012, **3**, 2262–2269.
213 G. Goddard, L. O. Brown, R. Habbersett, C. I. Brady, J. C. Martin, S. W. Graves, J. P. Freyer and S. K. Doorn, *J. Am. Chem. Soc.*, 2010, **132**, 6081–6090.
214 A. W. Wark, R. J. Stokes, S. B. Darby, W. E. Smith and D. Graham, *J. Phys. Chem. C*, 2010, **114**, 18115–18120.
215 T. A. Laurence, G. B. Braun, N. O. Reich and M. Moskovits, *Nano Lett.*, 2012, **12**, 2912–2917.
216 C. J. Murphy, T. K. San, A. M. Gole, C. J. Orendorff, J. X. Gao, L. Gou, S. E. Hunyadi and T. Li, *J. Phys. Chem. B*, 2005, **109**, 13857–13870.
217 P. R. Edwards, D. Sleith, A. W. Wark and R. W. Martin, *J. Phys. Chem. C*, 2011, **115**, 14031–14035.